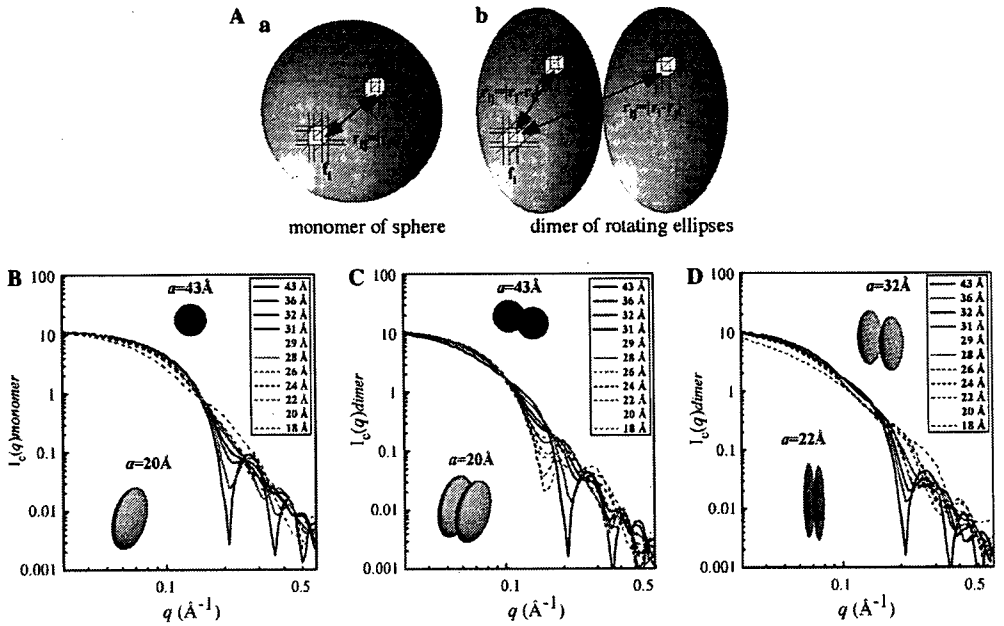

Fig. 3. Model calculations showing how ellipsoidal parameters affect the relative scattered intensity. (A) Schematic views of two body correlations. (a): monomer of a sphere. (b): dimer of rotating ellipses. In the q range of the SANS measurement, we assumed a constant scattering factor in the UCH-L1 variants, and thus divided the rotating ellipse by the resolution of a 5 Å cube. (B) $I_c(q)$ for the theoretical rotating ellipsoidal monomer, the remarks in the figure represent axis values of ellipsoid, e.g., when a is 20 Å, b and c are 62 Å. (C) $I_c(q)$ for the theoretical rotating ellipsoidal dimer (short axis, a; and long axis, b and c, $a \leqslant b = c$). (D) $I_c(q)$ for the theoretical rotating stick-like ellipsoidal dimer (short axis, a and b; and long axis, c, $a = b \leqslant c$), the remarks in the figure represent axis values of ellipsoid, e.g., When a and b are 22 Å, c is 164 Å. When a and b are 32 Å, c is 78 Å.

in the q range of 0.1–0.15 is observed on the SANS profiles of the rotating ellipsoidal dimers (short axis, a; and long axis, b and c, $a \leqslant b = c$), however, not observed on the rotating stick-like ellipsoidal dimer (short axis, a and b; and long axis, c, $a = b \leqslant c$) (Fig. 3D). The SANS profiles may provide the size of the rotating ellipsoidal dimers and therefore we applied this model to analyze the experimental SANS curves of UCH-L1 variants. The red lines in Fig. 4 are the best theoretical fits to a rotating ellipsoidal dimeric model determined individually for wild-type and each variant of UCH-L1s; the blue lines are those for a monomer having the same axis length. As shown in these figures, our data are consistent with this assumption in the q region. The wild-type is an ellipsoidal dimer [short axis, 29 Å; long axis, 52 Å (Fig. 4A)], the I93M mutant is also an ellipsoidal dimer [short axis, 20 Å; long axis, 62 Å (Fig. 4B)], the S18Y polymorphism is a spherical dimer [short axis, 43 Å; long axis, 43 Å (Fig. 4C)], and the I93M/S18Y double-substituted variant is an ellipsoidal dimer [short axis, 31 Å; long axis, 50 Å (Fig. 4D)]. The configuration of the aggregate was dependent on the monomeric protein structure caused by amino acid substitution. It is also quite clear that even the most deformed rotating ellipsoidal monomer never satisfies the experimental curve. The major component of UCH-L1 wild-type may exist as a dimer in water. These results imply that the most part of the wild-type and each UCH-L1 variant self-assembles and exists as a dimer in water. Thus, the fitting evaluation of the difference in the size and the shape between monomer and dimer is available by analyzing the SANS curve in the optimum q range.

To address whether the observed configurational differences of the UCH-L1 variants in water reflect on altered secondary structure, we used CD spectroscopy to estimate the secondary structure in the recombinant proteins (Fig. 5A). The ratios of α-helix, β-sheet, and other secondary structural features in these proteins were estimated from mean residue ellipticity data and are presented graphically in Fig. 5B. We previously indicated that relative to the wild-type, the I93M mutant displayed a slightly lower ellipticity over the range 195-200 nm, indicating a decreased α-helical content [24]. Relative to wild-type, the I93M substitution was also associated with the considerable increase in the content of β-sheet. On the other hand, the influence of the S18Y substitution on the variation of the secondary structures of UCHL-1 was smaller than that of I93M mutation, relative to the wild-type or the I93 mutant. However, the inclination was not only on the wild-type but also on the I93M mutant although the effect on increase of the β-turn content by the S18Y substitution of the amino acid sequence was small. These variations of the β-turn content were quite similar to those of the three-dimensional configuration of the ellipsoidal UCH-L1 based on SANS studies.

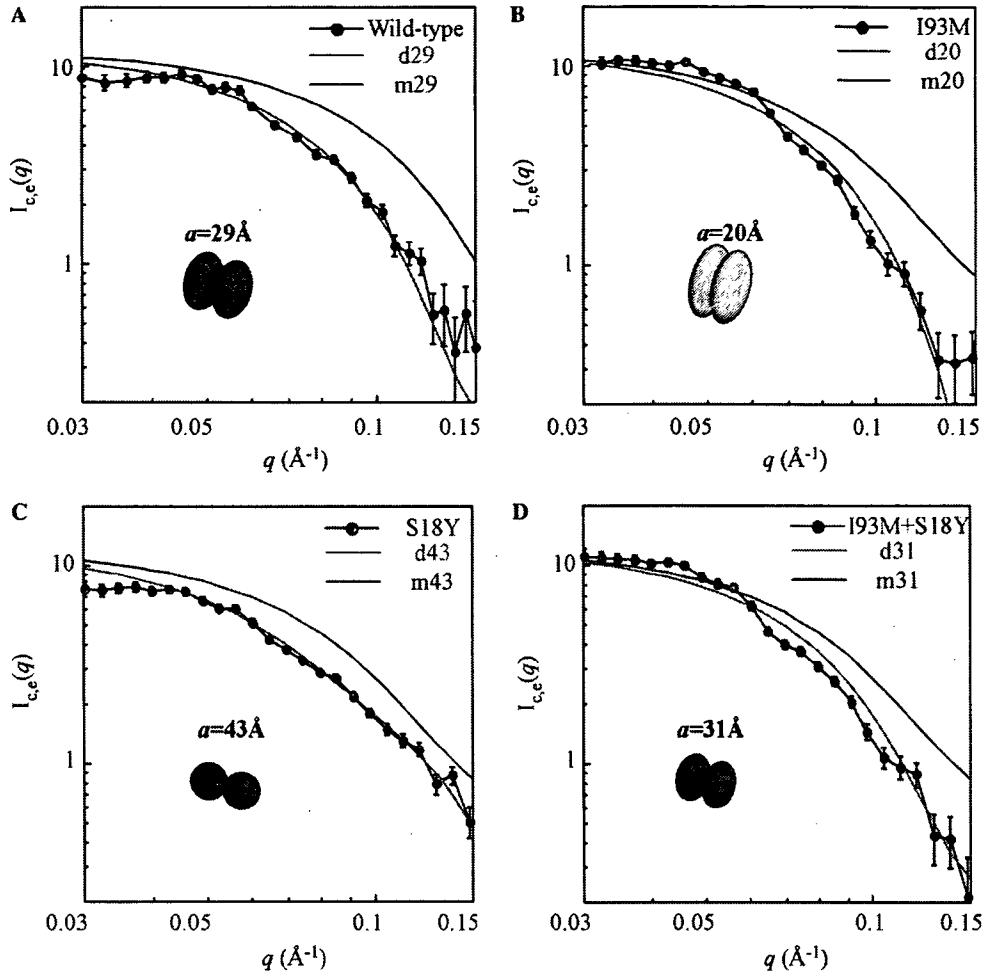

Fig. 4. Relative neutron scattering intensity $I(q)$ versus the magnitude of the scattering vector q. (A) $I_e(q)$ for the experimental curve of wild-type UCH-L1(black close circle). $I_c(q)$ for the calculated theoretical curves for dimer (d29) and monomer (m29). The red line corresponds to the theoretical fit for a rotating ellipsoidal dimer, (a, 29 Å; b, (=c), 52 Å). The blue line represents for a rotating ellipsoidal monomer having the same diameter. (B) $I_e(q)$ for the I93M mutant (black close circle). The red line corresponds to the theoretical fit for a rotating ellipsoidal dimer, (a, 20 Å, b, (=c), 62 Å). The blue line represents for the monomer. (C) $I_e(q)$ for the S18Y polymorphism (black close circle). The red line corresponds to the theoretical fit for a rotating spherical dimer, (a, 43 Å, b, (=c), 43 Å). The blue line represents for the monomer. (D) $I_e(q)$ for the I93M/S18Y double mutant (black close circle). The red line corresponds to the theoretical fit for rotating ellipsoidal dimer, (a, 31 Å, b, (=c), 50 Å). The blue line represents for the monomer.

Discussion

UCH-L1 is abundantly present neuronal brain protein enzyme with multiple enzymatic functions including hydrolysis of C-terminal ubiquityl esters, ubiquityl ligase activity, depending on multiple forms in an aqueous solution and stabilization of mono-ubiquitin. The aim of this study was to clarify whether UCH-L1 variants exist as a monomer or multimer in water and, in particular, to discuss the relation between the configuration of the variants and the risk of Parkinson's disease. We preferred SANS to address this question without adding any chemical modifications or physical force to proteins in water. We confirmed that no changes occurred on the SANS profiles of wild-type UCH-L1 and UCH-L1 variants during the measurement.

We first succeeded in demonstrating the configuration of UCH-L1 in an aqueous solution by SANS. The wild-type was a dimer, and the monomeric component was ellipsoidal, contrary to the expectation based on the crystal structure (Fig. 1C). The I93M variant was a dimer, and the monomeric component was more ellipsoidal than that of the wild-type. The protective polymorphic variant, S18Y, was also a dimer, but the configuration was quite different compared to wild-type and I93M, the monomeric component retained its spherical shape. The size-distribution of the UCH-L1 wild-type and variants is dependent on the concentration based on the time derivative analysis of the sedimentation velocity [16]. The 80% of the total wild-type is a monomer (~2.3S), ~15% is a dimer (4S), and ~5% is a tetramer (8S) at 7 μM. The populations of both oligomers increased with increased protein concentration, and the dimer became the predominant species at 70 μM. A similar concentration-dependent size growth was observed on S18Y; all of S18Y existed as a monomer at 10 μM, and

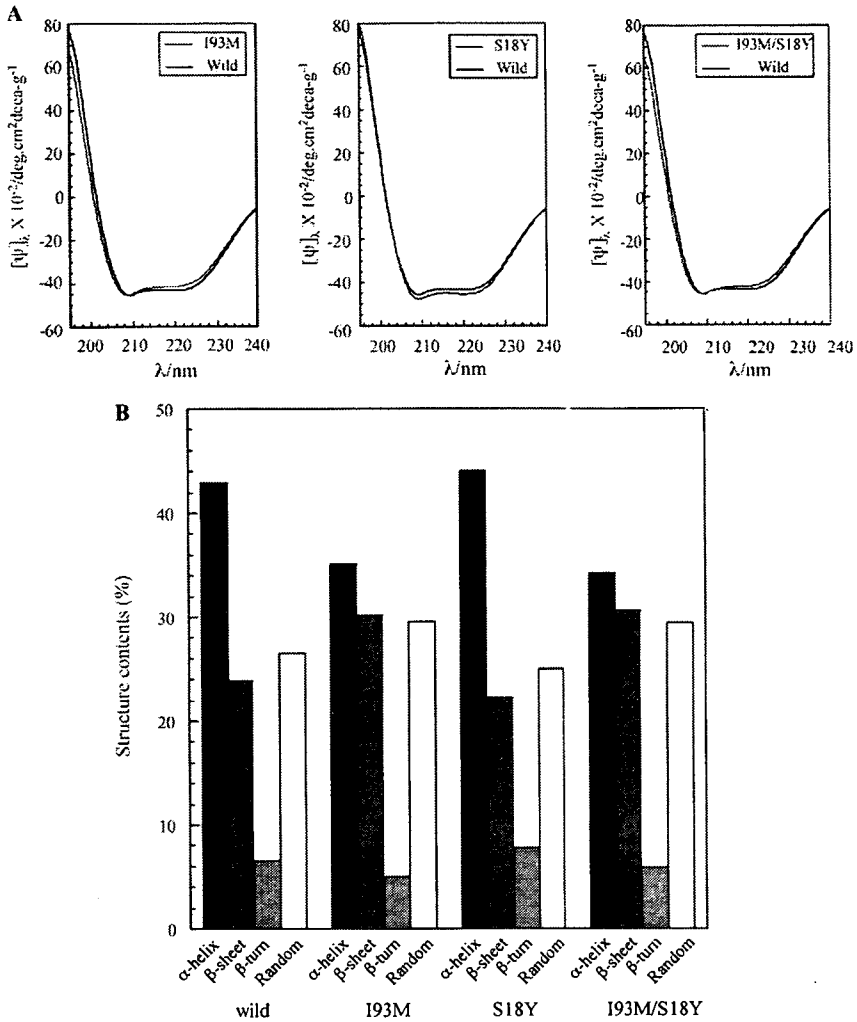

Fig. 5. CD spectra and secondary structural content of 6HN-tagged human UCH-L1s. CD spectra (mean residue ellipticity) for recombinant proteins (8.7×10^{-4} M) in a 20 mM Hepes buffer (pH 7.8). (A) Wild-type UCH-L1 is shown in black, I93M in red, S18Y in blue, and S18Y/I93M in green. (B) Secondary structural content of recombinant human 6HN-tagged UCH-L1s.

the dimer was detected at 28 μM. If homogeneity of the protein is attained in water, the configuration of protein should also be qualitatively equivalent at a lower concentration. Such an apparent size distribution was considered to be in a state of non-equilibrium, temporarily produced by adding a physical force, e.g., ultracentrifugation, to the protein.

In particular, we obtained important information about the shape of UCH-L1 in water by SANS observation; namely, the wild-type UCH-L1 and the variants formed rotating ellipsoids. The possible existence of the ellipsoidal dimer was suggested previously by analysis of the sedimentation velocity [16], indicating that the sedimentation value corresponding to the dimer (4S) was smaller than that of twice the monomer (~2.3S). This discordance implied that the dimer was anisotropic, but not a sphere. Here, we noted the influence of a comparative change of the β-turn content by the substitution of amino acid to the protein structure, because as is well known, the β-turn content is an important component for constructing a three-dimensional structure, i.e., the globularity of protein [33,34] despite the low content. The relationship between the relative change of globularity (circular ratio = a/b, see SANS data analysis) and that of β-turn content is summarized in Table 1. Based on the wild-type, I93M substitution decreases the circular ratio to 58% and the β-tune content to 76%, whereas S18Y substitution increased the circular ratio to 179% and the β-tune content to 118%. If the S18Y substitution occurs on the I93M mutant, the circular ratio increases to 193% and the β-turn also increases to 156%. Conversely, the circular ratio decreases to 52% and the β-turn also decreases to 64%, if an I93M substitution occurs on the S18Y polymorphism. An I93M mutation rendered the ellipsoidal dimer more stable because of a decrease of the α-helix [24], increase of the β-sheet, and decrease of the β-turn. Conversely, S18Y substitution regained the globu-

Table 1
Relation between the relative change of ellipsoidal and β-turn by amino acid substitution

Type	Amino acid substitution	Circular ratio	Relative change of ellipsoidal	β-turn content (%)	Relative change of β-turn
Wild	Non	1.8*	—	6.6	—
	I93M	3.1*	0.58[a]	5.0	0.76[d]
	S18Y	1.0*	1.79[a]	7.8	1.18[d]
I93M mutant	S18Y	1.6*	1.93[b]	5.8	1.56[e]
S18Y polymorphism	I93M	1.6*	0.52[c]	5.8	0.64[f]

[a] The relative changes of the circular ratio of I93M and S18Y were calculated based on the wild-type, [b]based on the I93M, and [c]based on the S18Y.
[d] The relative changes of the β-turn content of I93M and S18Y were calculated based on the wild-type, [e]based on the I93M, and [f]based on the S18Y.
* The relative change of the circular ratio (a/b) was calculated.

larity of the dimer, and resulted in changing the ellipsoidal form of wild-type up to spherical, and also the ellipsoidal form of the I93M mutant up to a similar circular ratio of wild-type. The globularity of UCH-L1 variants is closely related to the variation of the secondary structures, further, to the locations of the substitution of amino acids on the protein. The location of residue 93 is near the hydrolytic active site and the substitution may directly restructure the local geometric configuration and affect hydrolytic activity. On the other hand, although the location of residue 18 is distal from the active site, the position is on the hydrophilic surface of the protein and the substitution may often affect β-turn formation (Fig. 1C). When two protein molecules form a spherical dimer by a very weak attractive force, such as the S18Y polymorphism, the presence of this type of oligomer cannot be detected by other methods except by SANS. Thus, that the globularity of the UCH-L1 molecule depends on the β-turn content was responsible for not only the dimeric configuration, but also the risk of Parkinson's disease.

Finally, we considered the relationship between configuration of wild-type UCH-L1 and UCH-L1 variants and their functions, i.e., multiple enzymatic activities, C-terminal hydrolase, and ubiquityl ligase (Fig. 6) [15,16,19–24]. The progressive deformation of the ellipsoidal form by the I93M mutation simultaneously impaired both the hydrolytic and ubiquityl ligase activities. This configurational defect could cause impairment of dynamic flexibility, which is necessary for enzymatic functions by the enlargement of the hydrophobic region. We can surely imagine the relation between progressive deformation of ellipsoidal dimer caused by I93M mutation and impairment of enzymatic functions. The restoration of globularity of monomeric UCH-L1 by S18Y substitution augmented the hydrolytic activity. In contrast, it markedly decreased the ubiquityl ligase activity. However, it is not easy to imagine why the restoration of globularity by S18Y substitution simultaneously decreases ubiquityl ligase activity and increases hydrolytic activity. Hydrolysis may be the dominant activity of UCH-L1, but it seems to be very sensitive to the dimeric configuration. However, the ubiquityl ligase activity may vary, coupled with the hydrolytic one, if both active centers are adjoined. However, the increased hydrolase activity of the S18Y coupled with its decreased ligase

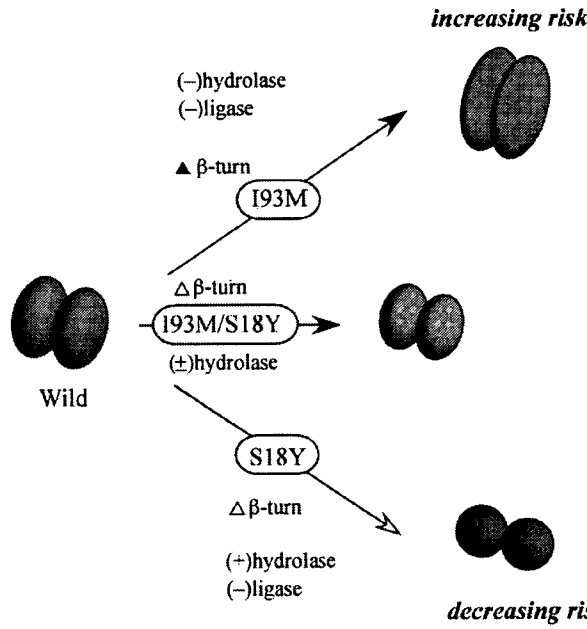

Fig. 6. Schematic speculative models of the relationship between the configuration of UCH-L1s in water and the multi-enzymatic activities. The self-assembled rotating ellipsoid wild-type dimer in water has both ubiquitin hydrolase activity and a ubiquityl ligase one. Both ubiquitin hydrolase and ubiquityl ligase activities decrease, as the result of an I93M mutation promoting the ellipsoidal deformation by a decrease of the β-turn and. A S18Y substitution recovers the globularity by an increase of the β-turn, causing an increase of ubiquitin hydrolase activity and a decrease of the ubiquityl ligase one. Thus, the variation of UCH-L1 hydrolytic activity caused by the deformation of the globularity of monomer component correlates to the PD risk.

activity (which can prevent α-synuclein degradation by K63-linked ubiquitin ligation) may be additive or synergistic with respect to the decreased risk of sporadic PD [16]. In this study, SANS observation may help in the confirmation of these hypotheses by observing either the hydrolytic digestion of ubiquitinated-proteins or oligomerization of free-ubiquitin based on the multiple enzymatic functions of PD-associated UCH-L1 variants. We demonstrated that SANS is an important technique for the direct observation of pathological protein assembly in water. We anticipate the design of a new SANS in the near future that is suitable for medical science and pathological analysis.

Acknowledgments

All authors acknowledge that the first two authors contributed equally to the study and are joint First Authors. This work was supported by Grants-in-Aid for Scientific Research from the Ministry of Health, Labour and Welfare of Japan, Grants-in-Aid for Scientific Research from the Ministry of Education, Culture, Sports, Science and Technology of Japan, a grant from Pharmaceuticals and Medical Devices Agency of Japan, and a grant from Japan Science and Technology Agency.

References

[1] M. Hirai, M. Koizumi, T. Hayakawa, H. Takahashi, S. Abe, H. Hirai, K. Miura, K. Inoue, Hierarchical map of protein unfolding and refolding at thermal equilibrium revealed by wide-angle X-ray scattering, Biochemistry 43 (2004) 9036–9049.

[2] Y. Yonezawa, S. Tanaka, T. Kubota, K. Wakabayashi, K. Yutani, S. Fujiwara, An insight into the pathway of the amyloid fibril formation of hen egg white lysozyme obtained from a small-angle X-ray and neutron scattering study, J. Mol. Biol. 323 (2002) 225–237.

[3] M. Hirai, H. Iwase, T. Hayakawa, K. Miura, K. Inoue, Structural hierarchy of several proteins observed by wide-angle solution scattering, J. Synchrotron Rad. 9 (2002) 202–205.

[4] M. Tehei, D. Madern, C. Pfister, G. Zacai, Fast dynamics of halophilic malate dehydrogenase and BSA measured by neutron scattering under various solvent conditions influencing protein stability, Proc. Natl. Acad. Sci. USA 98 (2001) 14356–14361.

[5] W.M. Garrison, Reaction mechanisms in the radiolysis of peptides, polypeptides, and proteins, Chem. Rev. 87 (1987) 381–389.

[6] S.D. Maleknia, C.Y. Ralston, M.D. Brenowitz, K.M. Downard, M.R. Chance, Millisecond radiolytic modification of peptides by synchrotron X-rays identified by mass spectrometry, Anal. Chem. 71 (1999) 3965–3973.

[7] G. Xu, M.R. Chance, Radiolytic modification of sulfur-containing amino acid residues in model peptides: fundamental studies for protein footprinting, Anal. Chem. 77 (2005) 2437–2449.

[8] S. Kuwamoto, S. Akiyama, T. Fujisawa, Radiation damage to a protein solution, detected by synchrotron X-ray small-angle scattering: dose-related considerations and suppression by cryoprotectant, J. Synchrotron Rad. 11 (2004) 462–468.

[9] F.F. Robert, D.J. Rodi, A. Mirza, T.C. Irving, E. Kondrashkinad, L. Makowski, High-resolution wide-angle X-ray scattering of protein solutions: effect of beam dose on protein integrity, J. Synchrotron Rad. 10 (2003) 398–404.

[10] F. Matumoto, K. Makiko, K. Maeda, H. Patzelt, Y. Maeda, S. Fujiwara, Conformational changes of troponin C within the thin filaments detected by neutron scattering, J. Mol. Biol. 342 (2002) 1209–1221.

[11] W. Yong, A. Lomakin, M.D. Kirkitadze, D.B. Teplow, S.-H. Chen, G.B. Benedek, Structure determination of micelle-like intermediates in amyloid-protein fibril assembly by using small angle neutron scattering, Proc. Natl. Acad. Sci. USA 99 (2002) 150–154.

[12] A.J. Doig, E. Hughes, R.M. Burke, T.J. Suã, R.K. Heenanå, J. Luã, Inhibition of toxicity and protofibril formation in the amyloid-β peptide β(25–35), Biochem. Soc. Trans. 30 (2002) 537–542.

[13] K. Lu, J. Jacob, P. Thiyagarajan, V.P. Conticello, D.G. Lynn, Exploiting amyloid fibril lamination for nanotube self-assembly, J. Am. Chem. Soc. 125 (2002) 6391–6393.

[14] K.D. Wilkinson, K.M. Lee, S. Deshpande, P. Duerksen-Hughes, J.M. Boss, J. Pohl, Ubiquitin and the Biology of the Cell, Plenum Press, New York, 1998, pp. 99–125.

[15] E. Leroy, R. Boyer, G. Auburger, B. Leube, G. Ulm, E. Mezey, G. Harta, M.J. Brownstein, S. Jonnalagada, T. Chernova, A. Dehejia, C. Lavedan, T. Gasser, P.J. Steinbach, K.D. Wilkinson, M.H. Polymeropoulos, The ubiquitin pathway in Parkinson's disease, Nature 395 (1998) 451–452.

[16] Y. Liu, H.A. Lashuel, A. Liu, P.T. Lansbury Jr., The UCH-L1 gene encodes two opposing enzymatic activities that affect a-synuclein degradation and Parkinson's disease susceptibility, Cell 111 (2002) 209–218.

[17] H. Osaka, Y.L. Wang, K. Takada, S. Takizawa, R. Setsuie, H. Li, Y. Sato, K. Nishikawa, Y.J. Sun, M. Sakurai, T. Harada, Y. Hara, I. Kimura, S. Chiba, K. Namikawa, H. Kiyama, M. Noda, S. Aoki, K. Wada, Ubiquitin carboxy-terminal hydrolase L1 binds to and stabilizes monoubiquitin ion neuron, Hum. Mol. Genet. 12 (2003) 1945–1958.

[18] Y. Manago, Y. Kanahori, A. Shimada, A. Sato, T. Amano, Y. Sato-Sano, R. Setsuie, M. Sakurai, S. Aoki, Y.-L. Wang, H. Osaka, K. Wada, M. Noda, Potentiation of ATP-induced currents due to activation of P2X receptors by ubiquitin carboxy-terminal hydrolase L1, J. Neurochem. 92 (2005) 1061–1072.

[19] D.M. Maraganore, M.J. Farrer, J.A. Hardy, S.J. Lincoln, S.K. McDonnell, W.A. Rocca, Case-control study of the ubiquitin carboxy-terminal hydrolase L1 gene in Parkinson s disease, Neurology 53 (1999) 1858–1860.

[20] P. Wintermeyer, R. Kruger, W. Kuhn, T. Muller, D. Woitalla, D. Berg, G. Becker, E. Leroy, M. Polymeropoulos, K. Berger, H. Przuntek, L. Schols, J.T. Epplen, O. Riess, Mutation analysis and association studies of the UCHL1 gene in German Parkinson's disease patients, Neuroreport 11 (2000) 2079–2082.

[21] J. Zhang, N. Hattori, E. Leroy, H.R. Morris, S. Kubo, T. Kobayashi, N.W. Wood, M.H. Polymeropoulos, Y. Mizuno, Association between a polymorphism of ubiquitin carboxyterminal hydrolase L1 (UCH-L1) gene and sporadic Parkinson's disease, Parkinsonism Relat. Disord. 6 (2000) 195–197.

[22] J. Satoh, Y. Kuroda, A polymorphic variation of serine to tyrosine at codon 18 in the ubiquitin C-terminal hydrolase-L1 gene is associated with a reduced risk of sporadic Parkinson's disease in a Japanese population, J. Neurol. Sci. 189 (2001) 113–117.

[23] Y. Momose, M. Murata, K. Kobayashi, M. Tachikawa, Y. Nakabayashi, I. Kanazawa, T. Toda, Association studies of multiple candidate genes for Parkinson s disease using single nucleotide polymorphisms, Ann. Neurol. 51 (2002) 133–136.

[24] K. Nishikawa, H. Li, R. Kawamura, H. Osaka, Y.L. Wang, Y. Hara, T. Hirokawa, Y. Manago, T. Amano, M. Noda, S. Aoki, K. Wada, Alterations of structure and hydrolase activity of parkinsonism-associated human ubiquitin carboxyl-terminal hydrolase L1 variants, Biochem. Biophys. Res. Commun. 304 (2003) 176–183.

[25] S.C. Johnston, C.N. Larsen, W.J. Cook, K.D. Wilkinson1, C.P. Hill, Crystal structure of a deubiquitinating enzyme (human UCH-L3) at 1.8 Å resolution, EMBO J. 16 (1997) 3787–3796.

[26] M.C. Peitsch, Protein modeling by E-mail, Bio/Technology 13 (1995) 658–660.

[27] N. Guex, M.C. Peitsch, SWISS-MODEL and the Swiss-Pdb Viewer: an environment for comparative protein modeling, Electrophoresis 18 (1997) 2714–2723.

[28] T. Schwede, J. Kopp, N. Guex, M.C. Peitsch, SWISS-MODEL: an automated protein homology-modeling server, Nucleic Acids Res. 31 (2003) 3381–3385.

[29] D.I. Svergun, C. Barberato, M.H.J. Koch, M. CRYSOL—a program to evaluate X-ray solution scattering of biological macromolecules from atomic coordinates, J. Appl. Crystallogr. 28 (1995) 768–773.

[30] D.I. Svergun, S. Richard, M.H.K. Koch, Z. Sayers, K.G. Zaccai, Protein hydration in solution: experimental observation by X-ray and neutron scattering, Proc. Natl. Acad. Sci. USA 95 (1998) 2267–2272.

[31] P. Debye, Zerstreuung von Rontgenstrahlen, Ann. Phys. 46 (1915) 809–823.

[32] J.T. Yang, C.S. Wu, H.M. Martinez, Calculation of protein conformation from circular dichroism, Methods Enzymol. 130 (1986) 208–269.

[33] R.H. Thomas, A.K. Roger, A.G. Margaret, F.G. John, O.F. Robert, Transfer of a b-turn structure to a new protein context, Nature 339 (1989) 73–76.

[34] A. Perezel, B.M. Foxman, G.D. Fasma, How reverse turns may mediate the formation of helical segments in proteins: an X-ray model, Proc. Natl. Acad. Sci. USA 89 (1992) 8210–8214.

Ubiquitin C-terminal hydrolase L1 regulates the morphology of neural progenitor cells and modulates their differentiation

Mikako Sakurai[1,2], Koichi Ayukawa[1], Rieko Setsuie[1,2], Kaori Nishikawa[1], Yoko Hara[1], Hiroki Ohashi[1,3], Mika Nishimoto[1,4], Toshiaki Abe[3], Yoshihisa Kudo[4], Masayuki Sekiguchi[1], Yae Sato[1,2], Shunsuke Aoki[1], Mami Noda[2] and Keiji Wada[1,*]

[1]Department of Degenerative Neurological Diseases, National Institute of Neuroscience, National Center of Neurology and Psychiatry, Kodaira, Tokyo, 187-8502, Japan
[2]Laboratory of Pathophysiology, Graduate School of Pharmaceutical Sciences, Kyushu University, Higashi-ku, Fukuoka, 812-8582, Japan
[3]Department of Neurosurgery, Graduate School of Medicine, Jikei University School of Medicine, Minato-ku, Tokyo, 105-8461, Japan
[4]Laboratory of Cellular Neurobiology, Tokyo University of Pharmacy and Life Science, Hachioji, Tokyo, 192-0392, Japan
*Author for correspondence (e-mail: wada@ncnp.go.jp)

Accepted 27 September 2005
Journal of Cell Science 119, 162-171 Published by The Company of Biologists 2006
doi:10.1242/jcs.02716

Summary

Ubiquitin C-terminal hydrolase L1 (UCH-L1) is a component of the ubiquitin system, which has a fundamental role in regulating various biological activities. However, the functional role of the ubiquitin system in neurogenesis is not known. Here we show that UCH-L1 regulates the morphology of neural progenitor cells (NPCs) and mediates neurogenesis. UCH-L1 was expressed in cultured NPCs as well as in embryonic brain. Its expression pattern in the ventricular zone (VZ) changed between embryonic day (E) 14 and E16, which corresponds to the transition from neurogenesis to gliogenesis. At E14, UCH-L1 was highly expressed in the ventricular zone, where neurogenesis actively occurs; whereas its expression was prominent in the cortical plate at E16. UCH-L1 was very weakly detected in the VZ at E16, which corresponds to the start of gliogenesis. In cultured proliferating NPCs, UCH-L1 was co-expressed with nestin, a marker of undifferentiated cells. In differentiating cells, UCH-L1 was highly co-expressed with the early neuronal marker TuJ1. Furthermore, when UCH-L1 was induced in nestin-positive progenitor cells, the number and length of cellular processes of the progenitors decreased, suggesting that the progenitor cells were differentiating. In addition, NPCs derived from *gad* (UCH-L1-deficient) mice had longer processes compared with controls. The ability of UCH-L1 to regulate the morphology of nestin-positive progenitors was dependent on its binding affinity for ubiquitin but not on hydrolase activity; this result was also confirmed using *gad*-mouse-derived NPCs. These results suggest that UCH-L1 spatially mediates and enhances neurogenesis in the embryonic brain by regulating progenitor cell morphology.

Key words: PGP9.5, UCH-L1, Nestin, Ubiquitin, Cell morphology, Differentiation, Progenitor

Introduction

Ubiquitin C-terminal hydrolase L1 (UCH-L1) is a member of the deubiquitylating enzymes and is one of the most abundant proteins in the brain. Whereas other UCH members are ubiquitously expressed, UCH-L1 is selectively expressed in neurons and testes/ovaries in the adult (Wilkinson et al., 1989). UCH-L1 is also known as PGP9.5 and is used as a neuron-specific marker in neuroanatomical and neuropathological studies (Dickson et al., 1994; McQuaid et al., 1995). Recent studies suggest that UCH-L1 is involved in neurodegeneration. The I93M mutation and the S18Y polymorphism in UCH-L1 are implicated in Parkinson's disease (Leroy et al., 1998; Satoh and Kuroda, 2001). Using gracile axonal dystrophy (*gad*) mice, we previously demonstrated that the dying-back type of axonal degeneration is caused by a deletion of the *Uchl1* gene (Saigoh et al., 1999). UCH-L1 has an affinity for ubiquitin and ensures its stability within neurons in vivo (Osaka et al., 2003). Furthermore, UCH-L1 has ubiquitin ligase activity (Liu et al., 2002). Thus, UCH-L1 might have multiple functions and more roles in biological phenomena than previously expected.

UCH-L1 mRNA is first detected at embryonic day (E) 8.5-9 in the neural tube and in the neural epithelium (Schofield et al., 1995). In addition, UCH-L1 immunoreactivity has been observed in the neural tube at E10.5 (Sekiguchi et al., 2003). However, its functional role in embryonic neurogenesis is not well understood. CDK5 and Dab1 are involved in regulating the migratory behavior of postmitotic neurons. Both p35, which is a CDK5 kinase, and Dab1 are degraded by the ubiquitin-proteasome pathway (Arnaud et al., 2003; Bock et al., 2004; Patrick et al., 1998). Thus, the ubiquitin system might be important in the migration and differentiation of postmitotic neurons and for the lamination pattern of the cerebral cortex.

Neural progenitor cells (NPCs) differentiate into neurons, astrocytes and oligodendrocytes (Qian et al., 1998; Qian et al., 2000; Shen et al., 1998). In the embryonic brain, neuroepithelial cells and radial glia are present in the ventricular zone (VZ); neurogenesis occurs first, followed by

gliogenesis. Committed progenitor cells move from the VZ to the cortical plate (CP) (Noctor et al., 2004). The differentiating cells migrate by means of radial migration, during which the migrating cells change their morphology (Kawauchi et al., 2003; Noctor et al., 2002; Tabata and Nakajima, 2003). Here, we analyzed the functional role of UCH-L1 using mouse embryonic NPCs. Our results indicate that UCH-L1 is expressed in nestin-positive NPCs and might regulate neurogenesis. The expression pattern of UCH-L1 changed in parallel with the transition from neuronal generation to glial generation. Furthermore, UCH-L1 modulated the length of nestin-positive processes in NPCs. Our results constitute the first evidence that UCH-L1 is important in neurogenesis and thus provide the basis for further investigation into the role of the ubiquitin system in neurogenesis.

Results

UCH-L1 expression in embryonic mouse brain

We first determined the specificity of the UCH-L1 antibody using immunoblotting (data not shown) and immunostaining. Because *gad* mice do not express endogenous UCH-L1 (Saigoh et al., 1999), we used these mice as a negative control. Heterozygous littermates had UCH-L1 immunostaining, whereas UCH-L1 immunoreactivity was not detected in the brains of *gad* mice (Fig. 1). These results confirmed the specificity of the antibody against UCH-L1. Using this antibody, we further compared the distribution and expression of UCH-L1 with the neural progenitor marker nestin and the early neuronal marker TuJ1. Nestin was expressed in the VZ of brains from both *gad* and heterozygous mice at E13 (Fig. 1). Nestin expression was observed throughout the region, whereas TuJ1 immunoreactivity was detected at the marginal zone (MZ). In heterozygous mice, UCH-L1 and nestin immunostaining overlapped in almost all cells in the VZ, suggesting that UCH-L1 is expressed in NPCs (Fig. 1A). TuJ1 expression colocalized with that of UCH-L1 in MZ cells, indicating that UCH-L1 is expressed in embryonic neurons as well (Fig. 1B). In E13 *gad* mouse brain, nestin staining differed compared with that in heterozygous littermates. Nestin staining was observed in many long radial fibers in the mutant, which we believed were radial glia; by contrast, staining in the heterozygotes occurred in radial glia as well as in neuronal cells at various stages of development (Fig. 1A; arrow and arrowhead).

We then looked for developmental changes in UCH-L1 expression. In the embryonic cerebral cortex, asymmetric cell division generates one neuron and one neural progenitor (Roegiers and Jan, 2004; Zhong et al., 1996; Zhong et al., 1997). These asymmetric cell divisions begin at E11, peak around E14, and subside after E16. At E14, astrocytes and oligodendrocytes are not yet present. However, at E16, glial cell production begins. The regional expression level for both nestin and TuJ1 did not change between E14 and E16 (Fig. 2A,B). At E14 and E16, nestin immunoreactivity was stronger in the VZ (Fig. 2A) and was faintly detected only along radial glial fibers in the CP (Fig. 2A,C; arrowhead) (Malatesta et al., 2003; Malatesta et al., 2000). TuJ1 immunoreactivity was predominantly detected in the MZ, CP, intermediate zone and subventricular zone at E14 and E16 (Fig. 2B,D). In the VZ, TuJ1 immunoreactivity was detected only in migrating neurons (Fig. 2D; arrowhead).

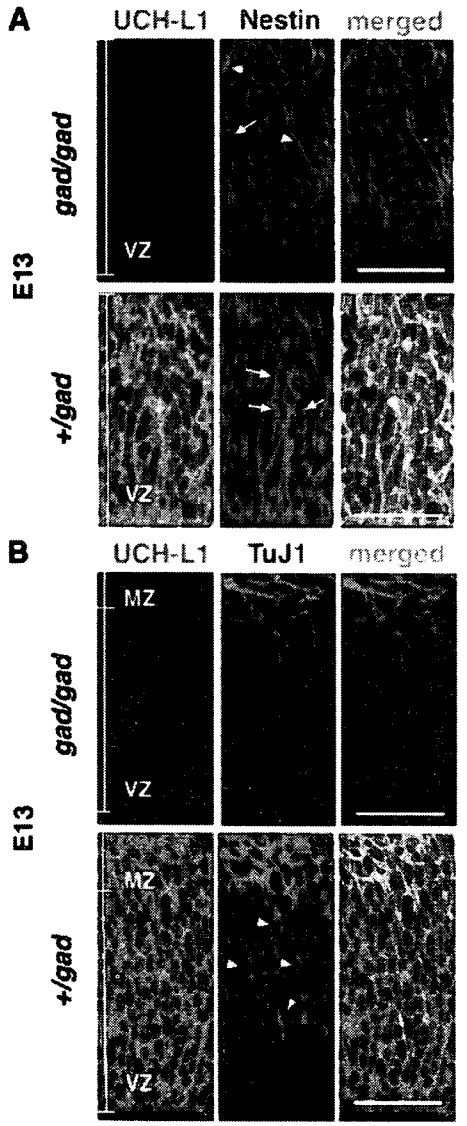

Fig. 1. Antibody specificity and expression of UCH-L1 in the ventricular zone at E13. UCH-L1 expression was detected using immunohistochemistry with anti-PGP9.5. UCH-L1 is not detected in the brain of *gad* mice at E13 (A,B) but is strongly expressed in heterozygous littermates (A,B). Confocal microscopic images of coronal sections of *gad* mice and heterozygous littermates were double stained with antibodies for the progenitor marker nestin and UCH-L1 (PGP9.5) (A) or for the early neuronal marker tubulin β III (TuJ1) and UCH-L1 (B). Long radial fibers are indicated by arrowheads, and various phases of progenitor cells are indicated by arrows (A). TuJ1-positive, migrating neuronal cells are indicated by arrowheads (B). MZ, marginal zone; VZ, ventricular zone. Bars, 40 μm.

By contrast, the pattern of UCH-L1 expression changed between E14 and E16 (Fig. 2A,B). At both stages of development, UCH-L1 was expressed in neuronal cells as well as in progenitor cells. UCH-L1 immunoreactivity was stronger in the VZ than in the CP at E14; however, the immunoreactivity

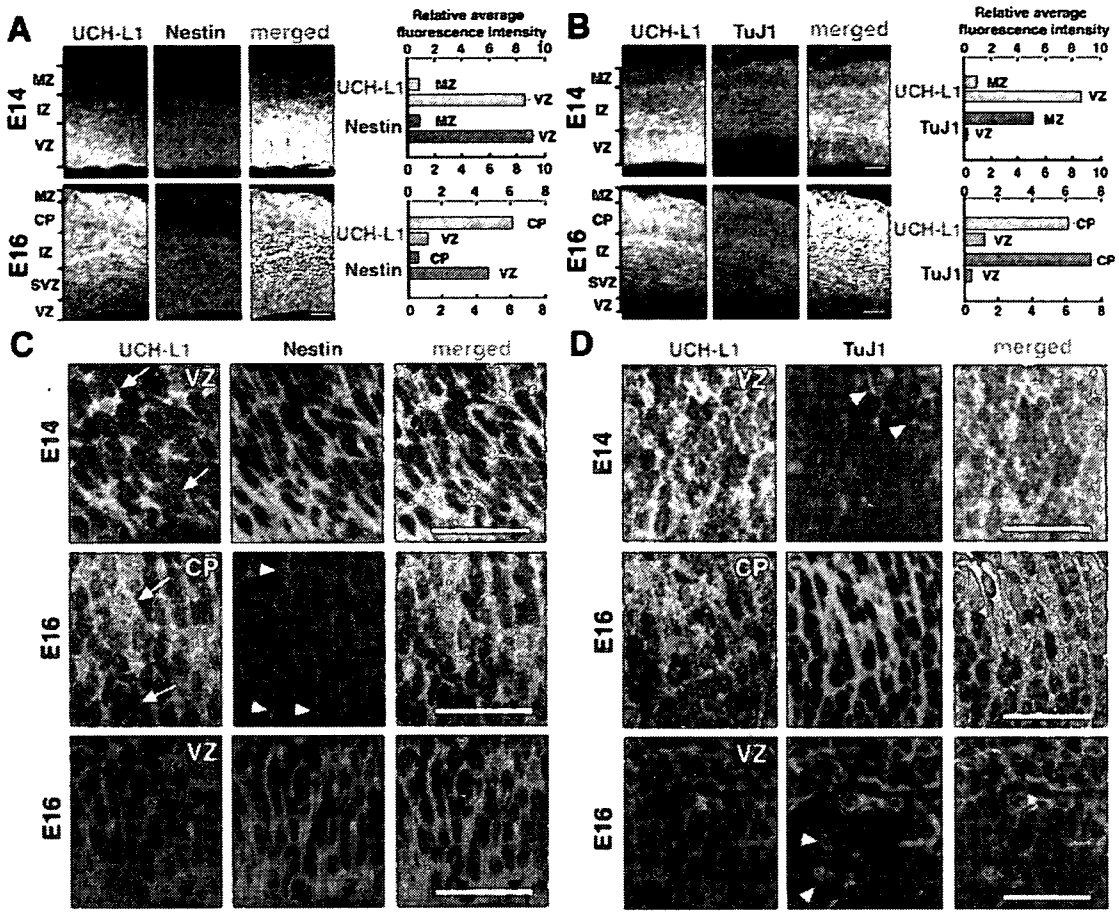

Fig. 2. Change in UCH-L1 expression pattern in the developing mouse brain. Cryosections of the brain at E14 and E16 were double stained with UCH-L1 and the neural progenitor marker nestin (A) or early neuronal marker TuJ1 (B). Unlike with UCH-L1, staining patterns for TuJ1 and nestin do not change between E14 and E16. At E14, UCH-L1 expression is higher in the VZ than in the MZ. At E16, higher expression of UCH-L1 is reciprocally detected in the CP. By contrast, at both E14 and E16, nestin is highly expressed in the VZ, and TuJ1 expression is higher in the MZ/CP. Fluorescence intensities per field (1700 μm^2) were measured in each layer of the E14 and E16 brain and are shown to the right. Bars, 80 μm. (C,D) Higher-magnification images from A,B of UCH-L1 expression in the E14 and E16 brain: UCH-L1 and nestin (C); UCH-L1 and TuJ1 (D). UCH-L1 and nestin are co-expressed in the VZ at E14 and E16. Nestin is expressed only in radial glial fibers (arrowheads) of the CP but not in neurons. UCH-L1 expression level is high. A representative cell with a high level of UCH-LI expression is indicated by a white arrow and one with low expression is indicated by a yellow arrow (C). An early neuronal marker, TuJ1, was expressed in both migrating (arrowheads) and mature neurons (D). CP, cortical plate; IZ, intermediate zone; MZ, marginal zone; SVZ, subventricular zone; VZ, ventricular zone. Bars, 40 μm.

was stronger in the CP than in the VZ at E16 (Fig. 2A,B). The regional change in UCH-L1 expression between E14 and E16 was further confirmed by measuring immunofluorescence intensities from confocal images of the MZ/CP and VZ. At E14, the relative UCH-L1 expression level in the VZ was 9.3 times higher than that in the MZ (Fig. 2A).

Conversely, at E16, when neuronal maturation occurs in the CP, UCH-L1 immunoreactivity in the CP was 5.0 times higher than in the VZ (Fig. 2B). UCH-L1 immunoreactivity colocalized with that of nestin in the VZ at both E14 and E16, although UCH-L1 expression in the VZ was lower at E16 (Fig. 2C). In the VZ at E14, nestin was expressed homogeneously; however, the pattern of UCH-L1 immunoreactivity was mixed, with strong and weak intensities (Fig. 2C; arrow). This expression pattern might reflect the heterogeneity of progenitor cells. Nestin-positive radial glial fibers were observed in the CP at E16 through mature neurons, which strongly expressed UCH-L1 (Fig. 2C) (Malatesta et al., 2000; Malatesta et al., 2003).

UCH-L1 and nestin expression in cultured NPCs

Because areas of nestin and UCH-L1 immunoreactivity overlapped in the VZ, where NPCs reside, we subsequently analyzed the transition of UCH-L1 expression using cultured NPCs. We performed double-labeling experiments for UCH-L1 and nestin expression in cultured NPCs. In the presence of basic fibroblast growth factor (bFGF), when NPCs are proliferating, the percentage of UCH-L1/nestin double-positive

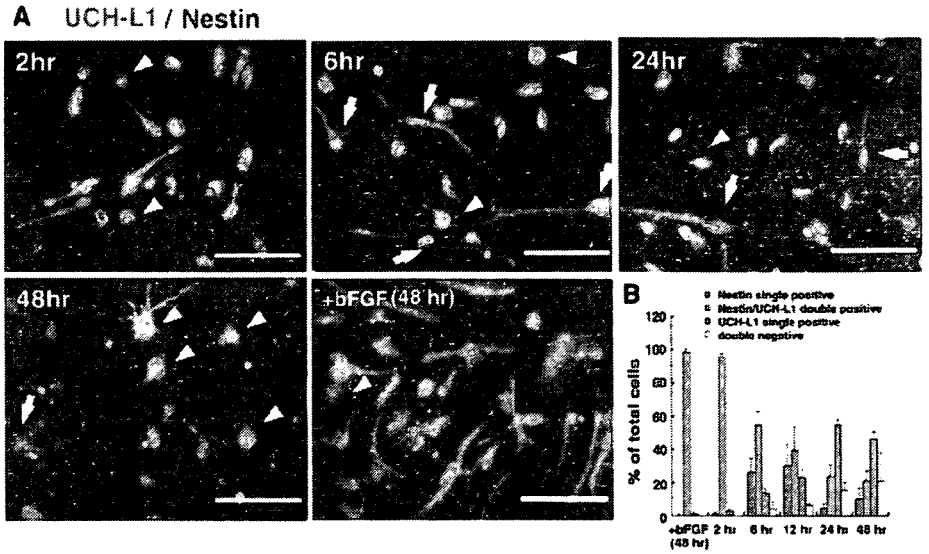

Fig. 3. Nestin and UCH-L1 expression in undifferentiated and differentiating NPCs at 2, 6, 12, 24 and 48 hours. (A) NPCs were immunolabeled with antibodies against nestin and UCH-L1 in the proliferating phase (+bFGF; at 48 hours) or the differentiation phase (–bFGF; 2, 6, 24, 48 hours). Cultures were counterlabeled with Hoechst nuclear dye to facilitate cell quantification. (B) Quantitative analysis of the percentage of cells stained with each antibody. Nestin-positive cells gradually decrease as differentiation proceeds. The UCH-L1 expression level is both high (arrowheads) and low (arrows) in nestin-positive cells at 6 hours. Each experiment was analyzed by counting cells in three independent wells at the indicated times. The experiments were repeated at least two times. Bars, 50 μm.

cells did not change 48 hours after plating, and almost all NPCs expressed UCH-L1 (Fig. 3A). The majority (97.5±2.2%; mean±s.d.) of cultured cells were nestin positive and most of them also stained for UCH-L1 2 hours after plating without bFGF, which triggers NPC differentiation. UCH-L1/nestin double-positive cells were detected at all time points, but as differentiation proceeded their numbers gradually decreased from 95.8±1.9% at 2 hours to 21.5±5.8% at 48 hours (Fig. 3A,B). Although UCH-L1 single-positive cells were rarely detected at 2 hours, the population increased with differentiation, and by 24 hours after bFGF removal 55.1±2.9% of cultured cells were UCH-L1 single-positive cells. Conversely, nestin single-positive cells were readily detected during the earlier phase of differentiation, especially at 6 hours (26.4±8.4% of total cells) and 12 hours (27.0±14.0% of total cells). The differentiating NPCs included nestin-positive cells in which UCH-L1 was either strongly or weakly expressed (Fig. 3A; arrow and arrowhead at 6 hours). These data indicate that UCH-L1 is expressed in progenitor cells as well as in differentiating NPCs. Nestin-positive cells can probably be

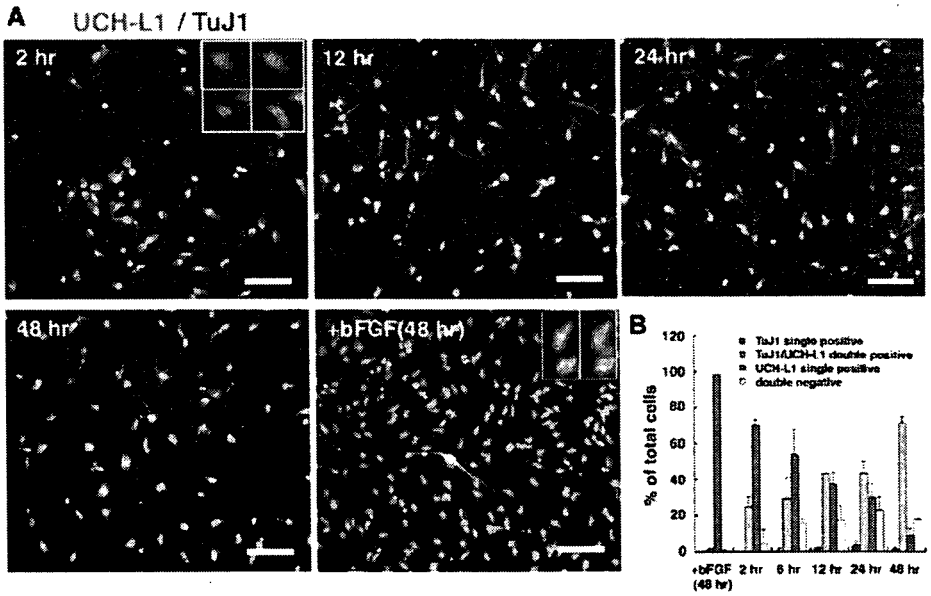

Fig. 4. UCH-L1 expression in neurogenesis. NPCs were immunolabeled with antibodies against TuJ1 and UCH-L1. Cultures were counterlabeled with Hoechst nuclear dye to facilitate cell quantification. Quantitative analysis of the percentage of cells stained with each antibody. (A) In the proliferating phase (+bFGF; at 48 hours) or the differentiation phase (–bFGF; 2, 12, 24, 48 hours), most TuJ1-positive cells co-express UCH-L1. The UCH-L1 expression level is both high and low in TuJ1-positive cells at 48 hours. (B) Quantitative analysis of the percentage of cells stained with each antibody. The number of TuJ1-positive cells gradually increased in the differentiating phase (–bFGF; B). Each experiment was analyzed by counting cells in three independent wells at the indicated times. The experiments were repeated at least two times. Bars, 50 μm.

categorized into at least two subgroups based on their UCH-L1 expression (Fig. 3A,B).

UCH-L1 and TuJ1 expression in cultured NPCs

We then analyzed the expression patterns of UCH-L1 and TuJ1. In the presence of bFGF, TuJ1-positive cells were rarely detected. However, in the absence of bFGF, TuJ1-positive cells were induced. In the cultures without bFGF, as the UCH-L1 single-positive cell population decreased with time, the UCH-L1/TuJ1 double-positive population increased (Fig. 4A,B). UCH-L1/TuJ1 double-negative cells were detected in the differentiating phases at 6, 12, 24 and 48 hours. UCH-L1/TuJ1 double-negative cells might be the nestin single-positive cells at 6 hours and 12 hours in Figs 3 and 4. TuJ1 single-positive cells were infrequently detected in the differentiating NPCs. Because 71.4±3.4% of NPCs differentiated into TuJ1-positive cells under our culture conditions without bFGF at 48 hours, almost all UCH-L1-positive cells are thought to differentiate into TuJ1-positive neuronal cells (Fig. 4A,B). The differentiating NPCs included TuJ1-positive cells in which UCH-L1 was either strongly or weakly expressed (Fig. 4A). These data indicate that UCH-L1-positive NPCs have a high potential for differentiating into neuronal cells and that TuJ1-positive neuronal cells are heterogeneous with regard to UCH-L1 expression.

Morphological classification of UCH-L1-positive NPCs

Nestin is a marker of undifferentiated cells, whereas UCH-L1 is a neuron-specific marker. Here, UCH-L1/nestin double-positive cells were present in cultured NPCs as well as in embryonic brain (Figs 2, 3). Cultured NPCs sequentially gave rise to neurons, then astrocytes, and finally oligodendrocytes (data not shown). Under our culture conditions, neurogenesis actively occurred in differentiating NPCs between 2 and 12 hours after plating (Fig. 4). Glial differentiation had not begun by this time. We collected differentiating NPCs at 6 hours and 12 hours after plating and then analyzed the morphology of nestin-positive cells (Fig. 5). Both UCH-L1/nestin double-positive cells and nestin single-positive cells were present in the population of differentiating NPCs. As the population of double-positive cells might represent a progression of differentiating neurons, we examined the morphology of these cells. Differentiating neurons undergo a stereotypical set of morphological changes, including length (from long to short) (Fukuda et al., 2003; Hartfuss et al., 2003; Nadarajah et al., 2001). We categorized the nestin-positive cells with respect to process length (long, short or round; Fig. 3). UCH-L1 single-positive and double-negative cells were included in the total number of cells. When the total length of processes was more than four times the diameter of the nucleus of the cell, the cell was categorized as 'long', whereas cells with shorter processes were categorized as 'short'. Cells that did not have processes were classified as 'round'. At 6 hours, the majority of nestin single-positive cells were long (18.2±7.6% vs 4.0±0.2% short cells; mean±s.d.; Fisher's PLSD, P=0.008), whereas the majority of UCH-L1/nestin double-positive cells were short (62.0±6.3%). This population was significantly greater than that of long cells (10.3±2.0%) and round cells (5.0±1.7%; Fisher's PLSD, P<0.0001). When NPCs with processes were subcategorized as unipolar, bipolar or multipolar, the unipolar population was significantly higher (62.3±16.9%) than the

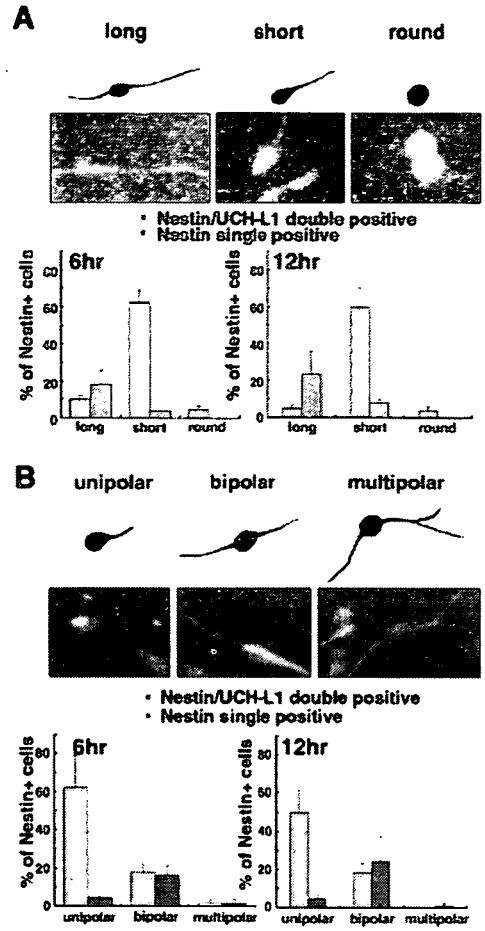

Fig. 5. Morphological identification of subpopulations of cultured NPCs at 6 and 12 hours after induction of differentiation. Differentiating NPCs were double stained with UCH-L1 and nestin. For the quantification depicted in A, differentiating NPCs stained with UCH-L1 and nestin were classified as long, short or round (see text). For the quantification depicted in B, differentiating NPCs were classified based on three kinds of cell morphology: unipolar, bipolar, or multipolar.

bipolar population (18.2±3.9%; Fisher's PLSD, P=0.002) in UCH-L1/nestin double-positive cells. Multipolar cells were not observed at 12 hours. However, in nestin single-positive cells, more NPCs were bipolar (16.5±4.6%) than unipolar (4.5±1.9%; Fisher's PLSD, P=0.009; Fig. 6B). Similar results were obtained at 12 hours (Fig. 6). Thus, most UCH-L1/nestin double-positive cells had shorter processes and were more likely to be unipolar.

Effect of UCH-L1 on nestin-positive processes

We next examined the effect of UCH-L1 on proliferating NPC morphology using the transient transfection method. NPCs were allowed to proliferate for 48 hours after transfection and were then induced to differentiate for 12 hours. The cells were fixed, and the length of nestin-positive processes was examined. To quantify the relationship between UCH-L1 expression and process formation, we measured the total length

of nestin-positive processes. Untransfected NPCs that were nestin positive had mainly long, bipolar processes (Fig. 3A, +bFGF). Cells that were transfected with a green fluorescent protein (GFP) expression vector (negative control) had a morphology that was similar to that of untransfected cells (Fig. 6A). By contrast, cells transfected with wild-type (WT) UCH-L1 cDNA had significantly shorter processes (47.6±6.4 μm, mean±s.e.m., n=81) than mock-transfected cells (69.9±7.0 μm, n=82) (Fig. 6A).

We then examined the relationship between the UCH-L1 structure and its activity with respect to morphological induction. We prepared two UCH-L1 mutants: D30A UCH-L1 lacked hydrolase activity and binding affinity for ubiquitin (Fig. 6B,C) (Osaka et al., 2003); C90S UCH-L1 lacked hydrolase activity but maintained binding affinity for ubiquitin (Fig. 6B,C) (Osaka et al., 2003). We compared the deubiquitylating activity of each UCH-L1 mutant using Ub-AMC as a substrate. The D30A mutant had little hydrolase activity, and the activity of the C90S mutant was not detectable (Fig. 6B; right). Sodium dodecyl sulfate-polyacrylamide gel electrophoresis revealed that there were no detectable contaminating proteins in these recombinant protein preparations (Fig. 6B; left). Co-immunoprecipitation experiments demonstrated that WT UCH-L1 and the C90S mutant physically associated with monoubiquitin. The D30A mutant (as well as GFP alone, which was used as a control) did not associate with ubiquitin (Fig. 6C). Although we did not detect a statistically significant difference, cells transfected with the D30A mutant tended to have longer nestin-positive processes (83.4±7.1 μm, n=87) as compared with cells transfected with the GFP expression vector (Fig. 6A). By contrast, cells transfected with the C90S mutant had significantly shorter fibers (39.3±4.5 μm, n=120; ANOVA: F=11.5, P<0.0001; Dunnett's multiple comparison test: GFP vs WT, P<0.05; GFP vs C90S, P<0.001; GFP vs D30A, P>0.05; Fig. 6A). We also compared the length of nestin-positive processes among UCH-L1 mutants (Bonferroni-Dunn Multiple Comparison Test: WT vs C90S, P=0.32; WT vs D30A, P<0.0001; D30A vs C90S, P<0.0001). Taken together, our data suggest that the effect of UCH-L1 expression on NPC morphology is dependent on the interaction between monoubiquitin and UCH-L1.

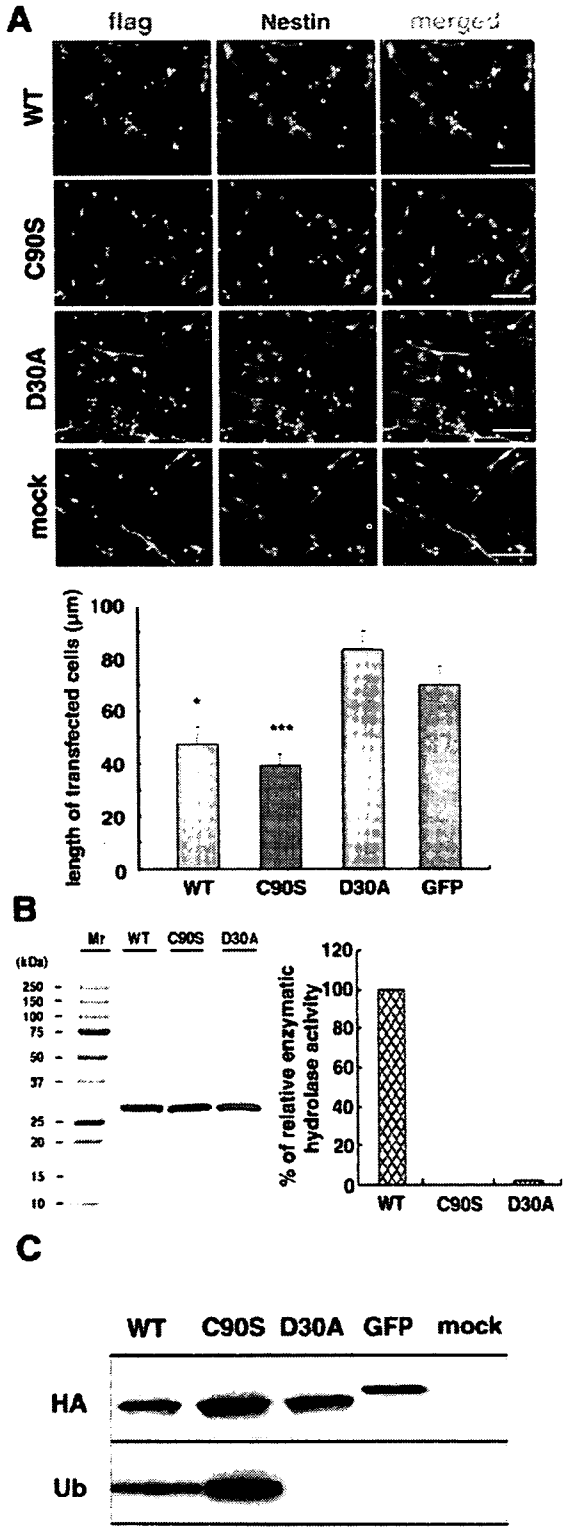

Fig. 6. The induction of short processes depends on the interaction between UCH-L1 and monoubiquitin. (A) FLAG-tagged WT UCH-L1, C90S UCH-L1, D30A UCH-L1 and GFP (all in the pCI-*neo* vector) were transfected into NPCs. Antibodies against the FLAG-tag were used to detect transfected UCH-L1. The green staining shows transfected cells and the red staining shows endogenous nestin. Transient transfection of each construct was performed under proliferating conditions. At 48 hours after transfection, bFGF was removed for 12 hours before the cultures were immunostained. The lengths of nestin-positive processes in immunostained cells were measured. Asterisks indicate differences from the value of GFP-transfected NPCs at *P<0.05 and ***P<0.001. Bars, 80 μm. (B) Visualization of recombinant 6HN-tagged UCH-L1 by sodium dodecyl sulfate-polyacrylamide gel electrophoresis with Coomassie staining (B, left). UCH-L1 hydrolase activity was measured by Ub-AMC hydrolysis. Enzyme concentration was 4.3 nM, and substrate concentration was 700 nM. Initial velocity data was used to determine the values for relative hydrolase activity of UCH-L1 (B, right). (C) UCH-L1 co-immunoprecipitated with Ub. Cytosolic extracts from NIH-3T3 cell lines stably expressing HA-tagged WT UCH-L1 and mutants thereof were immunoprecipitated using anti-HA and immunoblotted with anti-HA antibody or anti-Ub antibody.

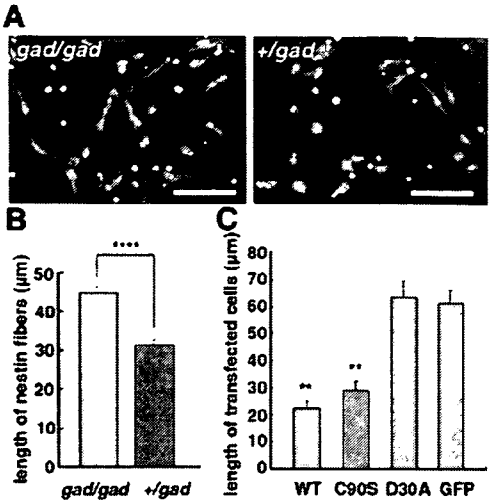

Fig. 7. A comparative experiment of *gad* mice and heterozygous littermates. The experiment compared *gad* mice (A,B) with a transfection study using FLAG-tagged WT UCH-L1, C90S UCH-L1, D30A UCH-L1 and GFP (mock) into *gad*-mouse-derived NPCs (C). The lengths of nestin-positive processes in immunostained cells were measured. NPCs from *gad* mice had longer nestin-positive processes compared with the control (A,B). (C) At 48 hours after transfection, bFGF was removed for 12 hours before the cultures were immunostained. The lengths of nestin-positive processes in immunostained cells were measured. Asterisks indicate differences from the value of GFP-transfected NPCs at $^{**}P<0.01$ and $^{****}P<0.0001$. Bar, 50 μm.

A comparative experiment using *gad*-mouse-derived NPCs

We did a comparative experiment using *gad* mice and heterozygous littermates. Nestin-positive NPCs from *gad* mice had longer processes. When we measured the length of nestin-positive fibers, NPCs from *gad* mice (45.0±1.4 μm, mean±s.e.m., n=366) had significantly longer nestin-positive processes compared with the control (31.4±1.3 μm, n=363) (Mann-Whitney U test: *gad* vs control, $P<0.0001$; Fig. 7A,B).

We next examined the effect of UCH-L1 on *gad*-mouse-derived NPCs using the transient transfection method. As observed in B6-derived cells, NPCs from *gad* mice that were transfected with WT UCH-L1 cDNA had significantly shorter processes (22.2±2.7 μm, mean±s.e.m., n=70) than mock-transfected cells (61.0±4.9 μm, n=88) (Bonferroni-Dunn multiple comparison test: GFP vs WT, $P<0.0001$) (Fig. 7C). Similarly, cells transfected with the C90S mutant had significantly shorter fibers (28.9±3.1 μm, n=71) (GFP vs C90S, $P<0.0001$). Although we did not detect a statistically significant difference, cells transfected with the D30A mutant tended to have longer nestin-positive processes (63.3±5.9 μm, n=80) as compared with cells transfected with the GFP expression vector (GFP vs D30A, P=0.70) (Fig. 7C). We also compared the length of nestin-positive processes among UCH-L1 mutants (Bonferroni-Dunn multiple comparison test: WT vs C90S, P=0.32; WT vs D30A, $P<0.0001$; D30A vs C90S, $P<0.0001$). Taken together, our data suggest that the effect of UCH-L1 expression on NPC morphology is dependent on the interaction between monoubiquitin and UCH-L1.

Discussion

UCH-L1 is a neuron-specific marker in the adult brain. In the present study, we provide experimental evidence that UCH-L1 is expressed in NPCs (Figs 2, 3). Using immunohistochemistry in the mouse brain, we detected UCH-L1 expression at E14 and E16. Interestingly, the expression pattern differed between E14 and E16 (Fig. 2). At E14, when the CP is forming, UCH-L1 expression was higher in the VZ than in the CP. At E14, the VZ contains progenitor cells that are generating neurons in the neocortex (Hashimoto and Mikoshiba, 2004; Malatesta et al., 2003). By contrast, UCH-L1 expression at E16 was lower in the VZ than in the CP. At E16, neuritogenesis and neuronal maturation are active in the CP, and gliogenesis is beginning in the VZ (Rice and Curran, 2001). The cerebral cortex layer becomes thicker at E16, where glial cells are not yet generated. The staining pattern for TuJ1 and nestin did not change between E14 and E16 (Fig. 2), indicating that UCH-L1 is highly expressed in the cortical layer prior to gliogenesis. The change in the expression pattern of UCH-L1 was coincident with the transition from neurogenesis to gliogenesis in the VZ. These results raise the possibility that UCH-L1 mediates not only the neuronal differentiation of NPCs but also the transition from neurogenesis to gliogenesis.

Time is a pivotal factor in the programmed sequence that produces neurons and glial cells from NPCs (Qian et al., 2000), in that the switch from neurogenesis to gliogenesis is regulated by time. The mechanism behind this progression of the progenitor cells is not well understood. Cultured NPCs generate neurons first, followed by astrocytes and then oligodendrocytes (Qian et al., 2000; Temple, 2001). This order of production for each population has been verified in vivo (Sauvageot and Stiles, 2002). The pattern of UCH-L1 immunoreactivity suggests that UCH-L1 is required for the onset of neurogenesis, which is followed by glial differentiation (Fig. 2).

We thus examined the role of UCH-L1 in neurogenesis using cultured NPCs. In UCH-L1/nestin double-staining experiments, the number of double-positive cells decreased with time in culture (Fig. 3). Conversely, UCH-L1 single-positive cells increased. In the double-staining experiments for UCH-L1 and TuJ1, the number of UCH-L1 single-positive cells decreased with time in culture, whereas the number of UCH-L1/TuJ1 double-positive cells increased (Fig. 4). These observations suggest that most UCH-L1-positive cells initially express nestin, but they express TuJ1 at a later stage. As we observed in vivo and in vitro (Figs 2-4), NPCs express UCH-L1, and its expression increases as the NPCs differentiate into neuronal cells. The number of nestin single-positive cells transiently increased before the UCH-L1 single-positive population increased (Fig. 3). The nestin single-positive population might have changed into the UCH-L1/nestin double-negative population (Fig. 3). Although the fate of the double-negative populations remains unknown, the double-negative cells might represent glial cells. Alternatively, some of the nestin single-positive cells might have changed into UCH-L1/nestin double-positive cells and then differentiated into UCH-L1 single-positive cells. A few UCH-L1-negative and TuJ1-positive cells were detected in the differentiating NPCs (Fig. 4). Thus, TuJ1-positive early neurons appear to be heterogeneous. UCH-L1/TuJ1 double-positive immunoreactivity suggested that UCH-L1 is not

absolutely required for some portion of neuronal cell development (Fig. 1B and Fig. 4A). This might explain why *gad* mouse neurons develop despite the absence of UCH-L1.

Because UCH-L1 was expressed in nestin-positive NPCs, we further examined the role of UCH-L1 in cell morphology (Fig. 5). Differentiating NPCs change morphology (Noctor et al., 2001), but the role of UCH-L1 in differentiating neurons has not been investigated. We classified nestin-positive cells based on the length of their processes. Nestin single-positive cells were predominantly long, whereas most UCH-L1/nestin double-positive cells were predominantly short (Fig. 5). These results suggest that UCH-L1 plays a role in regulating NPC process length. We examined this possibility by inducing UCH-L1 in nestin-positive cells. Untransfected, proliferating nestin-positive NPCs had mainly long and bipolar processes [Fig. 3A, bFGF (48 hours)], but when UCH-L1 was transfected, the length of nestin-positive NPC processes shortened (Fig. 6A). The unipolar population increased following UCH-L1 expression. These results support the idea that UCH-L1 regulates NPC morphology. This idea was further confirmed by observations in NPCs from *gad* mice; as shown in Fig. 7B, NPCs from homozygous *gad* mice had longer processes than those from heterozygous controls. In addition, we observed that transfection of UCH-L1 shortened the processes of NPCs from *gad* mice compared with mock transfectants (Fig. 7C).

Our results also suggest that at least two populations of NPCs exist in the embryonic brain. The populations can be classified by the presence or absence of UCH-L1. In the dentate gyrus of the adult mouse brain, there are two distinct subpopulations of nestin-positive cells (Fukuda et al., 2003): those having short processes differentiate into neurons, whereas those having long processes generate late progenitors, which have short processes. The nestin staining pattern of brains from *gad* mice differed from that of brains from heterozygous littermates (Fig. 1). In the *gad* mouse brain, nestin-positive radial fibers were prominent, and almost all progenitor cells appeared to have long processes (Fig. 1). Since UCH-L1 affected NPC morphology (Fig. 6A and Fig. 7C), the difference in vivo indicates that differentiation itself was modulated by the absence of UCH-L1. Considering that neurons are present in the *gad* mouse even though it lacks UCH-L1 expression, further investigation into the morphological role of UCH-L1 using various approaches including the BrdU studies should provide important information about the heterogeneity of cortical neurons.

UCHs hydrolyze ubiquitin C-terminal small adducts in vitro (Larsen et al., 1998). Recently, a significant relationship was reported between UCH-L1 hydrolase activity and cell proliferation in lung cancer cell lines (Liu et al., 2003). We previously demonstrated that UCH-L1 extends ubiquitin half-life and prevents ubiquitin degradation. This function depends on the interaction between UCH-L1 and monoubiquitin but not on hydrolase activity (Osaka et al., 2003). In the present study, WT UCH-L1 and the C90S mutant both decreased the length of NPC processes. Both molecules associate with monoubiquitin, unlike another mutant, D30A, which did not affect process length (Fig. 6). Similar results were obtained from the transfection study using nestin-positive NPCs from *gad* mice (Fig. 7C). Thus, the effect of UCH-L1 on NPC process length is dependent on the interaction between UCH-L1 and ubiquitin but not on hydrolase activity. Although we did not examine the ligase activity of each mutant (Liu et al., 2002), the C90S mutant is unlikely to have ligase activity, because conjugation of ubiquitin to the C90S mutant forms a stable complex that prevents the release of ubiquitin (Sullivan and Vierstra, 1993). This observation suggests that the ligase activity is not related to the morphological changes that occurred in NPCs.

The ubiquitin system has an essential role in various physiological events, including cell-cycle progression, specific gene transcription, membrane protein trafficking, reversal of stress damage and intracellular signaling (Weissman, 2001). In cortical neurogenesis, the role of the ubiquitin system is not well understood. Several molecules that are important in cortical neurogenesis, including Notch, P35 and Dab1, are ubiquitylated (Arnaud et al., 2003; Bock et al., 2004; Patrick et al., 1998; Qiu et al., 2000). Here we show for the first time that UCH-L1 is expressed in NPCs and regulates their morphology. In addition, in vivo UCH-L1 expression is localized to the VZ and cortical layers that are undergoing neurogenesis. Cells undergoing gliogenesis had little UCH-L1 expression in vivo. These results suggest that UCH-L1 facilitates neurogenesis, an activity that appears to depend on the affinity of UCH-L1 for ubiquitin.

Materials and Methods

Animals

Pregnant C57BL/6J mice were purchased from CLEA Japan. The *gad* mouse is an autosomal recessive mutant that was obtained by crossing CBA and RFM mice (Saigoh et al., 1999). The *gad* line was maintained by intercrossing for more than 20 generations (Kwon et al., 2003; Saigoh et al., 1999). All animal experiments were performed in the laboratory according to the NIH Standards for Treatment of Laboratory Animals.

Antibodies and reagents

Monoclonal and polyclonal antibodies used in this study were as follows: monoclonal anti-nestin antibody (Becton Dickinson; and Rat401, Developmental Studies Hybridoma Bank, The University of Iowa, Iowa City, IA), monoclonal anti-neuronal tubulin β III antibody (TuJ1; Covance), polyclonal anti-UCH-L1 antibody (PGP9.5; RA95101, UltraClone), and polyclonal anti-FLAG antibody (Sigma). All secondary polyclonal antibodies conjugated to Alexa Fluor fluorescein were purchased from Molecular Probes.

Cortical NPC culture and differentiation conditions in C57BL/6 mice

Cortical NPCs were cultured as previously described (Nakashima et al., 1999). Briefly, embryos were removed from pregnant C57BL/6J mice (CLEA Japan) and staged according to morphological criteria to confirm the gestational day (Kaufman et al., 1998). Developing mouse cerebral cortex was dissected from E14 embryos. Cells were mechanically dissociated by trituration and plated at a concentration of 3.0×10^6 cells per 10 cm dish (Becton Dickinson) precoated with 10 ml of 15 μg/ml poly-L-ornithine (Sigma) and 10 ml of 1 μg/ml fibronectin (Nitta Gelatin). Cells were expanded for 5 days in serum-free neurobasal (NB) medium (Invitrogen) supplemented with B27 (Invitrogen), 0.5 mM L-glutamine (Invitrogen), 100 U/ml penicillin and 100 μg/ml streptomycin (Invitrogen). This medium contained 10 ng/ml bFGF (PeproTech). Cultures were maintained at 37°C in an atmosphere of 95% air and 5% CO_2. For secondary culture, bFGF-expanded NPCs were washed in warm Hank's Balanced Salt Solution, detached with mechanical pipetting, and resuspended in NB medium supplemented with B27, but not bFGF. Cells were then replated in 24-well plates (Nunc; 1.8×10^5 cells per well) that were precoated with 500 μl of 15 μg/ml poly-L-ornithine and 500 μl of 1 μg/ml fibronectin for immunofluorescence staining at each time point.

Cortical NPC culture and differentiation conditions in *gad* mice

Culture of NPCs derived from *gad* mice was performed as with NPCs derived from B6 mice. Developing mouse cerebral cortex was dissected from embryos at E13.5 to E14.5. The precise gestational day was determined according to previously established morphological criteria (Kaufman et al., 1998). NPCs from each embryo were collected and cultured separately. Each genotype was determined later using PCR and, as a result, each pair of *gad* and control littermate mice from two sets of

parents were used. Each culture of NPCs was replated in 24-well plates without bFGF and stained using anti-UCH-L1 24 hours after plating.

Immunohistochemistry

Brain sections were stained as previously described (Li et al., 2003; Osaka et al., 2003). Briefly, E14 and E16 mouse brains were removed and fixed in 4% paraformaldehyde/phosphate-buffered saline (PBS) for 2 hours at room temperature, cryoprotected in 30% sucrose in PBS and frozen in dry ice. Sections (20 μm thick) were cut on a cryostat, and mounted on aminopropylsilane (APS)-coated glass slides. They were then washed three times in PBS for 5 minutes, and blocked for 1 hour at room temperature with 3% bovine serum albumin, 2% (v/v) normal goat serum, and 0.2% (v/v) Triton X-100 in PBS (pH 7.4). Sections were incubated with primary antibodies [anti-nestin antibody (Rat401) 1:10; or anti-UCH-L1 antibody (RA95101) 1:4000; or anti-TuJ1 antibody, 1:1000] overnight at 4°C or for 2 hours at room temperature. After rinsing in PBS, the sections were incubated for 2 hours with diluted fluorescein-conjugated secondary antibody (1:200). The images were obtained with a confocal laser scanning TCS SL microscope, and detailed analyses were performed using an LSC confocal microscope system (Leica). Immunofluorescence intensities were measured from confocal images with Mac SCOPE software (version 2.59; Mitani).

Immunocytochemistry

Cells were stained as previously described (Aoki et al., 2002). Briefly, all incubations and washes were performed at room temperature. Cells were fixed with 3.8% formaldehyde/PBS for 10 minutes and permeabilized with 0.02% (v/v) Triton X-100/PBS for 5 minutes. Fixed cells were blocked with 3.3% goat serum for 30 minutes. Cells were incubated with a diluted primary polyclonal or monoclonal antibody (both were used for double staining) for 0.5-1 hour. The cells were then incubated with diluted secondary antibody conjugated to fluorescein for 0.5-1 hour. Antibody dilutions were as follows: anti-UCH-L1 antibody, 1:4000; anti-nestin antibody, 1:500; anti-TuJ1, 1:500. All secondary antibodies were diluted 1:200 in 1% goat serum/PBS before use. The images were obtained with fluorescence microscopy on an IX70 microscope (Olympus).

Transfection

For C57BL/6 mice, cells replated in 24-well plates were cultured overnight in growth medium containing bFGF and B27. The next day, each construct was transfected using Lipofectamine 2000 (Invitrogen) according to the manufacturer's instructions. NPCs were allowed to proliferate for 48 hours after transfection and then induced to differentiate for 12 hours without bFGF. For *gad*-mouse-derived NPCs, transfection was done in a similar manner.

Expression plasmids for human UCH-L1 variants

Mutant cDNAs encoding human UCH-L1 containing either the D30A or C90S substitution were obtained using the QuikChange site-directed mutagenesis kit (Stratagene) with the following mutagenesis oligonucleotides: 5′-CAGTGG-CGCTTCGTGGCCGTGCTGGGGCTGGAAG-3′ and 5′-CTTCCAGCCCCAG-CACGGCCACGAAGCGCCACTG-3′ for D30A; 5′-CCATTGGGAATTCCTCT-GGCACAATCGGAC-3′ and 5′-GTCCGATTGTGCCACAGGAATTCCCAA-TGG-3′ for C90S. Each single-nucleotide mutation in the resulting plasmids was confirmed by sequencing. Mammalian expression plasmids containing either FLAG-tagged human WT UCH-L1 or the D30A or C90S mutants were constructed using a pCI-*neo* mammalian expression vector (Promega). Bacterial expression plasmids containing either 6HN-tagged human WT UCH-L1 or the D30A or C90S mutants were constructed using a tetracycline-inducible expression system. *Xho*I-*Not*I cDNA fragments of the pCI-*neo* WT UCH-L1 or the D30A and C90S mutants and constructs were digested, and the DNA fragments were ligated between the *Sal*I and *Not*I sites in pPROtetE233 (Clontech) to generate pPROtetE233 6HN-tagged human WT, D30A and C90S UCH-L1 vectors. These expression plasmids were confirmed by sequencing.

In vitro assay for human UCH-L1 activity

Purified human UCH-L1 and the fluorogenic substrate ubiquitin-7-amino-4-methylcoumarin (Ub-AMC; Boston Biochem) were used to determine steady-state kinetic parameters as described previously (Nishikawa et al., 2003).

Immunoprecipitation

NIH-3T3 cells stably expressing human WT UCH-L1 or the C90S or D30A mutants, all with an HA-FLAG double tag at the N terminus, were cultured to subconfluency in a 10 cm dish, lyzed with 1 ml of modified RIPA buffer [50 mM Tris-HCl, pH 7.5, 1% (v/v) NP-40, 0.25% sodium deoxycholate, 150 mM NaCl, 1 mM EDTA] with EDTA-free complete protease inhibitor cocktail (Roche), sonicated and centrifuged at 18,000 *g* for 20 minutes at 4°C. Immunoprecipitation was performed as described previously (Ogawa et al., 2002).

Statistics

Statistical analyses were performed using StatView, version 5.0 (SAS) and Prism, version 3 (GraphPad Software). Analysis of variance (ANOVA) was used to assess differences between groups. A P value of less than 0.05 was considered statistically significant. When ANOVA results were statistically significant, they were examined by Fisher's PLSD, or Dunnett's multiple comparison test, or Bonferroni-Dunn multiple comparisons post hoc test. Differences between *gad* mice and control mice were analyzed using the Mann-Whitney U test.

The authors thank Yuh Nung Jan and Hua-Shun Li for providing the immunohistochemistry methods; Yoshihiro Nakatani and Hidesato Ogawa for providing the retroviral expression system and immunoprecipitation methods; and Masako Shikama for the care and breeding of animals. This work was supported by Grants-in-Aid for Scientific Research from the Ministry of Health, Labour and Welfare of Japan, and Grants-in-Aid for Scientific Research from the Ministry of Education, Culture, Sports, Science and Technology of Japan.

References

Aoki, S., Su, Q., Li, H., Nishikawa, K., Ayukawa, K., Hara, Y., Namikawa, K., Kiryu-Seo, S., Kiyama, H. and Wada, K. (2002). Identification of an axotomy-induced glycosylated protein, AIGP1, possibly involved in cell death triggered by endoplasmic reticulum-Golgi stress. *J. Neurosci.* **22**, 10751-10760.

Arnaud, L., Ballif, B. A. and Cooper, J. A. (2003). Regulation of protein tyrosine kinase signaling by substrate degradation during brain development. *Mol. Cell. Biol.* **23**, 9293-9302.

Bock, H. H., Jossin, Y., May, P., Bergner, O. and Herz, J. (2004). Apolipoprotein E receptors are required for reelin-induced proteasomal degradation of the neuronal adaptor protein Disabled-1. *J. Biol. Chem.* **279**, 33471-33479.

Dickson, D. W., Schmidt, M. L., Lee, V. M., Zhao, M. L., Yen, S. H. and Trojanowski, J. Q. (1994). Immunoreactivity profile of hippocampal CA2/3 neurites in diffuse Lewy body disease. *Acta Neuropathol. (Berl.)* **87**, 269-276.

Fukuda, S., Kato, F., Tozuka, Y., Yamaguchi, M., Miyamoto, Y. and Hisatsune, T. (2003). Two distinct subpopulations of nestin-positive cells in adult mouse dentate gyrus. *J. Neurosci.* **23**, 9357-9366.

Hartfuss, E., Forster, E., Bock, H. H., Hack, M. A., Leprince, P., Luque, J. M., Herz, J., Frotscher, M. and Gotz, M. (2003). Reelin signaling directly affects radial glia morphology and biochemical maturation. *Development* **130**, 4597-4609.

Hashimoto, M. and Mikoshiba, K. (2004). Neuronal birthdate-specific gene transfer with adenoviral vectors. *J. Neurosci.* **24**, 286-296.

Kaufman, M. H., Brune, R. M., Davidson, D. R. and Baldock, R. A. (1998). Computer-generated three-dimensional reconstructions of serially sectioned mouse embryos. *J. Anat.* **193**, 323-336.

Kawauchi, T., Chihama, K., Nabeshima, Y. and Hoshino, M. (2003). The in vivo roles of STEF/Tiam1, Rac1 and JNK in cortical neuronal migration. *EMBO J.* **22**, 4190-4201.

Kwon, J., Kikuchi, T., Setsuie, R., Ishii, Y., Kyuwa, S. and Yoshikawa, Y. (2003). Characterization of the testis in congenitally ubiquitin carboxy-terminal hydrolase-1 (Uch-L1) defective (gad) mice. *Exp. Anim.* **52**, 1-9.

Larsen, C. N., Krantz, B. A. and Wilkinson, K. D. (1998). Substrate specificity of deubiquitinating enzymes: ubiquitin C-terminal hydrolases. *Biochemistry* **37**, 3358-3368.

Leroy, E., Boyer, R., Auburger, G., Leube, B., Ulm, G., Mezey, E., Harta, G., Brownstein, M. J., Jonnalagada, S., Chernova, T. et al. (1998). The ubiquitin pathway in Parkinson's disease. *Nature* **395**, 451-452.

Li, H. S., Wang, D., Shen, Q., Schonemann, M. D., Gorski, J. A., Jones, K. R., Temple, S., Jan, L. Y. and Jan, Y. N. (2003). Inactivation of Numb and Numblike in embryonic dorsal forebrain impairs neurogenesis and disrupts cortical morphogenesis. *Neuron* **40**, 1105-1118.

Liu, Y., Fallon, L., Lashuel, H. A., Liu, Z. and Lansbury, P. T., Jr (2002). The UCH-L1 gene encodes two opposing enzymatic activities that affect alpha-synuclein degradation and Parkinson's disease susceptibility. *Cell* **111**, 209-218.

Liu, Y., Lashuel, H. A., Choi, S., Xing, X., Case, A., Ni, J., Yeh, L. A., Cuny, G. D., Stein, R. L. and Lansbury, P. T., Jr (2003). Discovery of inhibitors that elucidate the role of UCH-L1 activity in the H1299 lung cancer cell line. *Chem. Biol.* **10**, 837-846.

Malatesta, P., Hartfuss, E. and Gotz, M. (2000). Isolation of radial glial cells by fluorescent-activated cell sorting reveals a neuronal lineage. *Development* **127**, 5253-5263.

Malatesta, P., Hack, M. A., Hartfuss, E., Kettenmann, H., Klinkert, W., Kirchhoff, F. and Gotz, M. (2003). Neuronal or glial progeny: regional differences in radial glia fate. *Neuron* **37**, 751-764.

McQuaid, S., McConnell, R., McMahon, J. and Herron, B. (1995). Microwave antigen retrieval for immunocytochemistry on formalin-fixed, paraffin-embedded post-mortem CNS tissue. *J. Pathol.* **176**, 207-216.

Nadarajah, B., Brunstrom, J. E., Grutzendler, J., Wong, R. O. and Pearlman, A. L. (2001). Two modes of radial migration in early development of the cerebral cortex. *Nat. Neurosci.* **4**, 143-150.

Nakashima, K., Yanagisawa, M., Arakawa, H., Kimura, N., Hisatsune, T., Kawabata, M., Miyazono, K. and Taga, T. (1999). Synergistic signaling in fetal brain by STAT3-Smad1 complex bridged by p300. *Science* **284**, 479-482.

Nishikawa, K., Li, H., Kawamura, R., Osaka, H., Wang, Y. L., Hara, Y., Hirokawa, T., Manago, Y., Amano, T., Noda, M. et al. (2003). Alterations of structure and

hydrolase activity of parkinsonism-associated human ubiquitin carboxyl-terminal hydrolase L1 variants. *Biochem. Biophys. Res. Commun.* **304**, 176-183.

Noctor, S. C., Flint, A. C., Weissman, T. A., Dammerman, R. S. and Kriegstein, A. R. (2001). Neurons derived from radial glial cells establish radial units in neocortex. *Nature* **409**, 714-720.

Noctor, S. C., Flint, A. C., Weissman, T. A., Wong, W. S., Clinton, B. K. and Kriegstein, A. R. (2002). Dividing precursor cells of the embryonic cortical ventricular zone have morphological and molecular characteristics of radial glia. *J. Neurosci.* **22**, 3161-3173.

Noctor, S. C., Martinez-Cerdeno, V., Ivic, L. and Kriegstein, A. R. (2004). Cortical neurons arise in symmetric and asymmetric division zones and migrate through specific phases. *Nat. Neurosci.* **7**, 136-144.

Ogawa, H., Ishiguro, K., Gaubatz, S., Livingston, D. M. and Nakatani, Y. (2002). A complex with chromatin modifiers that occupies E2F- and Myc-responsive genes in G0 cells. *Science* **296**, 1132-1136.

Osaka, H., Wang, Y. L., Takada, K., Takizawa, S., Setsuie, R., Li, H., Sato, Y., Nishikawa, K., Sun, Y. J., Sakurai, M. et al. (2003). Ubiquitin carboxy-terminal hydrolase L1 binds to and stabilizes monoubiquitin in neuron. *Hum. Mol. Genet.* **12**, 1945-1958.

Patrick, G. N., Zhou, P., Kwon, Y. T., Howley, P. M. and Tsai, L. H. (1998). p35, the neuronal-specific activator of cyclin-dependent kinase 5 (Cdk5) is degraded by the ubiquitin-proteasome pathway. *J. Biol. Chem.* **273**, 24057-24064.

Qian, X., Goderie, S. K., Shen, Q., Stern, J. H. and Temple, S. (1998). Intrinsic programs of patterned cell lineages in isolated vertebrate CNS ventricular zone cells. *Development* **125**, 3143-3152.

Qian, X., Shen, Q., Goderie, S. K., He, W., Capela, A., Davis, A. A. and Temple, S. (2000). Timing of CNS cell generation: a programmed sequence of neuron and glial cell production from isolated murine cortical stem cells. *Neuron* **28**, 69-80.

Qiu, L., Joazeiro, C., Fang, N., Wang, H. Y., Elly, C., Altman, Y., Fang, D., Hunter, T. and Liu, Y. C. (2000). Recognition and ubiquitination of Notch by Itch, a hect-type E3 ubiquitin ligase. *J. Biol. Chem.* **275**, 35734-35737.

Rice, D. S. and Curran, T. (2001). Role of the reelin signaling pathway in central nervous system development. *Annu. Rev. Neurosci.* **24**, 1005-1039.

Roegiers, F. and Jan, Y. N. (2004). Asymmetric cell division. *Curr. Opin. Cell Biol.* **16**, 195-205.

Saigoh, K., Wang, Y. L., Suh, J. G., Yamanishi, T., Sakai, Y., Kiyosawa, H., Harada, T., Ichihara, N., Wakana, S., Kikuchi, T. et al. (1999). Intragenic deletion in the gene encoding ubiquitin carboxy-terminal hydrolase in gad mice. *Nat. Genet.* **23**, 47-51.

Satoh, J. and Kuroda, Y. (2001). A polymorphic variation of serine to tyrosine at codon 18 in the ubiquitin C-terminal hydrolase-L1 gene is associated with a reduced risk of sporadic Parkinson's disease in a Japanese population. *J. Neurol. Sci.* **189**, 113-117.

Sauvageot, C. M. and Stiles, C. D. (2002). Molecular mechanisms controlling cortical gliogenesis. *Curr. Opin. Neurobiol.* **12**, 244-249.

Schofield, J. N., Day, I. N., Thompson, R. J. and Edwards, Y. H. (1995). PGP9.5, a ubiquitin C-terminal hydrolase; pattern of mRNA and protein expression during neural development in the mouse. *Brain Res. Dev. Brain Res.* **85**, 229-238.

Sekiguchi, S., Yoshikawa, Y., Tanaka, S., Kwon, J., Ishii, Y., Kyuwa, S., Wada, K., Nakamura, S. and Takahashi, K. (2003). Immunohistochemical analysis of protein gene product 9.5, a ubiquitin carboxyl-terminal hydrolase, during placental and embryonic development in the mouse. *Exp. Anim.* **52**, 365-369.

Shen, Q., Qian, X., Capela, A. and Temple, S. (1998). Stem cells in the embryonic cerebral cortex: their role in histogenesis and patterning. *J. Neurobiol.* **36**, 162-174.

Sullivan, M. L. and Vierstra, R. D. (1993). Formation of a stable adduct between ubiquitin and the Arabidopsis ubiquitin-conjugating enzyme, AtUBC1+. *J. Biol. Chem.* **268**, 8777-8780.

Tabata, H. and Nakajima, K. (2003). Multipolar migration: the third mode of radial neuronal migration in the developing cerebral cortex. *J. Neurosci.* **23**, 9996-10001.

Temple, S. (2001). The development of neural stem cells. *Nature* **414**, 112-117.

Weissman, A. M. (2001). Themes and variations on ubiquitylation. *Nat. Rev. Mol. Cell. Biol.* **2**, 169-178.

Wilkinson, K. D., Lee, K. M., Deshpande, S., Duerksen-Hughes, P., Boss, J. M. and Pohl, J. (1989). The neuron-specific protein PGP 9.5 is a ubiquitin carboxyl-terminal hydrolase. *Science* **246**, 670-673.

Zhong, W., Feder, J. N., Jiang, M. M., Jan, L. Y. and Jan, Y. N. (1996). Asymmetric localization of a mammalian numb homolog during mouse cortical neurogenesis. *Neuron* **17**, 43-53.

Zhong, W., Jiang, M. M., Weinmaster, G., Jan, L. Y. and Jan, Y. N. (1997). Differential expression of mammalian Numb, Numblike and Notch1 suggests distinct roles during mouse cortical neurogenesis. *Development* **124**, 1887-1897.

Journal of Cell Science

American Journal of Pathology, Vol. 169, No. 1, July 2006

DOI: 10.2353/ajpath.2006.060085

Cell Injury, Repair, Aging and Apoptosis

Photoreceptor Cell Apoptosis in the Retinal Degeneration of *Uchl3*-Deficient Mice

Yae Sano,*† Akiko Furuta,* Rieko Setsuie,*† Hisae Kikuchi,* Yu-Lai Wang,* Mikako Sakurai,*† Jungkee Kwon,*‡ Mami Noda,† and Keiji Wada*

From the Department of Degenerative Neurological Diseases, National Institute of Neuroscience, National Center of Neurology and Psychiatry, Tokyo, Japan; the Laboratory of Pathophysiology,† Graduate School of Pharmaceutical Sciences, Kyushu University, Fukuoka, Japan; and the Laboratory of Animal Medicine,‡ College of Veterinary Medicine, Chonbuk National University, Jeonju, Korea*

UCH-L3 belongs to the ubiquitin C-terminal hydrolase family that deubiquitinates ubiquitin-protein conjugates in the ubiquitin-proteasome system. A murine *Ucbl3* deletion mutant displays retinal degeneration, muscular degeneration, and mild growth retardation. To elucidate the function of UCH-L3, we investigated histopathological changes and expression of apoptosis- and oxidative stress-related proteins during retinal degeneration. In the normal retina, UCH-L3 was enriched in the photoreceptor inner segment that contains abundant mitochondria. Although the retina of *Uchl3*-deficient mice showed no significant morphological abnormalities during retinal development, prominent retinal degeneration became manifested after 3 weeks of age associated with photoreceptor cell apoptosis. Ultrastructurally, a decreased area of mitochondrial cristae and vacuolar changes were observed in the degenerated inner segment. Increased immunoreactivities for manganese superoxide dismutase, cytochrome *c* oxidase I, and apoptosis-inducing factor in the inner segment indicated mitochondrial oxidative stress. Expression of cytochrome c, caspase-1, and cleaved caspase-3 did not differ between wild-type and mutant mice; however, immunoreactivity for endonuclease G was found in the photoreceptor nuclei in the mutant retina. Hence, loss of UCH-L3 leads to mitochondrial oxidative stress-related photoreceptor cell apoptosis in a caspase-independent manner. Thus, *Uchl3*-deficient mice represent a model for adult-onset retinal degeneration associated with mitochondrial impairment. *(Am J Pathol 2006, 169:132–141; DOI: 10.2353/ajpath.2006.060085)*

The ubiquitin system has been implicated in numerous cellular processes, including protein quality control, cell cycle, cell proliferation, signal transduction, membrane protein internalization, and apoptosis.[1,2] Ubiquitin-dependent processes are regulated by ubiquitinating enzymes, E1, E2, and E3, and deubiquitinating enzymes such as ubiquitin-specific proteases and ubiquitin C-terminal hydrolases (UCHs).[1,3–5] To date, four isozymes of UCHs, UCH-L1, UCH-L3, UCH-L4, and UCH-L5, have been cloned in mouse or human.[6–8] UCH-L1, also known as PGP 9.5, has been well characterized among the isozymes. UCH-L1 is selectively localized to brains and testis/ovaries[7] and functions as a ubiquitin ligase in addition to a deubiquitinating enzyme.[9] Furthermore, two distinct mutations are linked to Parkinson's disease in human[10] and gracile axonal dystrophy (*gad*) in mice.[11] UCH-L3, on the other hand, displays 52% amino acid identity to UCH-L1.[12] Uchl3 mRNA is expressed throughout various tissues and is especially enriched in testis and thymus.[13] In addition to its ubiquitin hydrolase activity, *in vitro* studies indicate that UCH-L3 cleaves the C terminus of the ubiquitin-like protein Nedd-8.[14,15] Although UCH-L1 and UCH-L3 are suggested to function as reciprocal modulators of germ cell apoptosis in experimental cryptorchid testis,[16] the cellular localization and function of UCH-L3 remain unknown in other organs.

Recently, *Uchl3*-deficient mice were generated with a deletion of exons 3 to 7, which are essential for hydrolase

Supported by grants-in-aid for scientific research from the Japan Society for the Promotion of Science; for priority area research from the Ministry of Education, Culture, Sports, Science and Technology, Japan; Kyushu University Foundation for Scientific Research from the Ministry of Health, Labour and Welfare, Japan; and the program for Promotion of Fundamental Studies in Health Sciences from the National Institute of Biomedical Innovation, Japan.

Accepted for publication March 23, 2006.

Address reprint requests to Akiko Furuta, M.D., Ph.D., Department of Degenerative Neurological Diseases, National Institute of Neuroscience, National Center of Neurology and Psychiatry, 4-1-1, Ogawahigashi, Kodaira, Tokyo 187-8502, Japan. E-mail: afuruta@ncnp.go.jp.

activity.[13] These mutant mice display postnatal retinal and muscular degenerations as well as mild growth retardation.[17] Retinal development is morphologically normal, but progressive retinal degeneration is reported to be evident at 3 months after birth.[17] However, precise chronological changes and the mechanism of the retinal degeneration in *Uchl3*-deficient mice has not been studied.

Both the caspase-dependent pathway and the caspase-independent pathway have been proposed to be involved in the models of retinal degeneration, including model animals for retinitis pigmentosa (such as Royal College of Surgeons (RCS) rat and retinal degeneration (*rd*) mice),[18] retinal detachment,[19] light injury,[20,21] ischemic injury,[22] and age-related macular degeneration.[23] In the ubiquitin system, UCH-L1 is involved in ischemia-induced apoptosis in the inner retina.[24] The role of UCH-L3 in retinal degeneration, however, is unclear.

To elucidate the function of UCH-L3, we investigated the histopathological changes and protein expression with respect to apoptotic pathways in *Uchl3*-deficient mice. Our results show that UCH-L3 is mainly localized to the photoreceptor inner segment that contains abundant mitochondria in the normal retina. *Uchl3*-deficient mice displayed caspase-independent apoptosis during postnatal retinal degeneration associated with increased expression of the markers for mitochondrial oxidative stress at the inner segment. We propose a possible antiapoptotic role of UCH-L3 in photoreceptor cells.

Materials and Methods

Animals

We used age-matched *Uchl3*-deficient mice and wild-type mice, all of which were offspring male from 15 to 20 pairs of heterozygotes that had been backcrossed with C57BL/6J at postnatal ages of 0 days (P0), 10 days (P10), 3 weeks (3w), 6 weeks (6w), 8 weeks (8w), and 12 weeks (12w). The total number of wild-type and *Uchl3*-deficient mice examined in the present study was 79, of which 30 mice were used for Western blotting, 42 mice were used for hematoxylin and eosin staining, immunohistochemistry, and terminal deoxynucleotidyl transferase-mediated dUTP nick end labeling (TUNEL) assay, and 7 mice were used for electron microscopy. The mice were maintained at the National Institute of Neuroscience, National Center of Neurology and Psychiatry (Tokyo, Japan). The experiments using the mice were approved by the Institute's Animal Investigation Committee.

Western Blotting

Eyes from P10-, 3w-, and 6w-old mice of both genotypes (10 mice in each time point, for a total of 30 mice) were lysed in protein lysis buffer (100 mmol/L Tris-HCl, pH 8.0, 300 mmol/L NaCl, 2% Triton X-100, 0.2% SDS, 2% sodium deoxycholate, 2 mmol/L EDTA) containing protease inhibitor (Complete protease inhibitor cocktail; Sigma-Aldrich, St. Louis, MO). The amount of total protein of each sample was determined by the Bio-Rad protein assay (Bio-Rad, Hercules, CA) using bovine serum albumin as a standard. Total protein (50 μg/lane) was separated by 15% SDS-polyacrylamide gels (Perfect NT Gel, DRC, Tokyo, Japan). Proteins were transferred to immuno-Blot polyvinylidene difluoride membranes (Bio-Rad) and incubated with 5% skim milk in TBST (50 mmol/L Tris-HCl-buffered saline, pH 7.0, containing 0.05% Triton X-100) for 1 hour at room temperature. The membranes were incubated with a 1:1000 dilution of each primary antibody for UCH-L1, UCH-L3,[25] and β-actin (1:1000; Sigma-Aldrich) overnight at 4°C. For the preparation of anti-mouse UCH-L1 antibody, histidine-tagged mouse UCH-L1 (6His-mUCH-L1) was prepared as described previously[26] and used to generate a polyclonal antiserum in rabbit (Takara, Tokushima, Japan). The polyclonal antibody was purified by affinity chromatography. The specificity of this antibody to the mouse UCH-L1 was verified by Western blotting using brain lysates from *gad* mice and wild-type mice (data not shown). The membranes were washed in TBST and further incubated with antimouse or rabbit IgG-horseradish peroxidase conjugate (1:1000; Chemicon, Temecula, CA). After washing in TBST, the membranes were developed with the Super Signal West Dura or Femto Extended Duration Substrate (Pierce, Rockford, IL) and analyzed with a ChemiImager (Alpha Innotech, San Leandro, CA). Western blotting was performed five times per each antibody.

Morphometric Analysis and Immunohistochemistry of Retina

Mice of both genotypes at P0, P10, 3w, 6w, 8w, and 12w of age (7 mice in each time point, total of 42 mice) were deeply anesthetized with diethylether, decapitated, and the eyes removed, immersion-fixed with 4% paraformaldehyde overnight at 4°C, and embedded in paraffin wax. Deparaffinized sections were stained with hematoxylin and eosin and examined under an Axioplan2 microscope (Carl Zeiss, Oberkochen, Germany) at a magnification ×400, and the thickness of each layer was measured using WinRoof software (Mitani Shoji, Tokyo, Japan).

For immunohistochemical studies, 5-μm-thick sagittal sections at the level of the optic nerve were deparaffinized and treated with 1% hydrogen peroxide (H_2O_2) for 30 minutes, incubated with 1% skim milk in phosphate-buffered saline (PBS, pH 7.4) for 1 hour at room temperature followed by incubation overnight at 4°C with each primary antibody for UCH-L1 and UCH-L3[25] diluted 1:500 in 1% skim milk in PBS. To characterize apoptosis- and oxidative stress-related proteins, antibodies to the following proteins were used; apoptosis-inducing factor (AIF; 1:500, Chemicon), caspase-1 (1:100; Cell Signaling Technology, Beverly, MA), caspase-3 (1:1000; Cell Signaling Technology), cleaved caspase-3 (1:50; Cell Signaling Technology), cytochrome *c* (1:1000; Santa Cruz Biotechnology, Santa Cruz, CA), cytochrome *c* oxidase I

(COX, 1:10,000; Molecular Probes, Eugene, OR), endonuclease G (Endo G; 1:500, Chemicon) and manganese superoxide dismutase (Mn-SOD; 1:10,000, Stressgen, Victoria, BC, Canada). The sections were washed in PBS and then incubated with biotinylated secondary antibodies diluted 1:500 in PBS containing 1% skim milk. The sections were treated with the VECTASTAIN Elite ABC kit (Vector Laboratories, Burlingame, CA) according to the manufacturer's protocol and developed with 0.02% 3,3'-diaminobenzidine tetrahydrochloride solution containing 0.003% H_2O_2. After visualization, sections were counterstained with hematoxylin. Sections were examined with an Axioplan2 microscope (Carl Zeiss). Immunohistochemistry was performed in at least three repeated experiments. The relative immunoreactivity for COX, Mn-SOD, AIF, and Endo G in each layer of mutant mice was compared with that of wild-type mice and was classified into no change (−), slight increase (±), mild increase (+), and marked increase (++).

TUNEL Staining

Apoptotic cells were examined in mice of both genotypes at P0, P10, 3w, 6w, 8w, and 12w (7 mice in each time point, for a total of 42 mice) by TUNEL stain using the Dead-End Fluorimetric TUNEL system kit (Promega, Madison, WI) according to the manufacturer's instructions. The sections were examined by using a confocal laser scanning microscope (Olympus, Tokyo, Japan). The microphotographs were captured at magnification ×400 (0.066 mm^2/each retinal section), positive cells were counted (Fluoview 2.0; Olympus), and the data were subjected to statistical analysis.

Electron Microscopic Analysis

3w-old mice of both genotypes (total 7 mice) were deeply anesthetized with 20% chloral hydrate aqueous solution and perfused with the following fixative: 2% paraformaldehyde, 2% glutaraldehyde in PBS, or sodium cacodylate buffer (pH 7.4). The eyes were removed and postfixed with the same fixative overnight at 4°C. The posterior segments of eyes were trimmed and washed with PBS or sodium cacodylate buffer, incubated in phosphate-buffered 1% osmium tetroxide for 1 hour, and dehydrated in ethanol and embedded in Epon 812 resin (TAAB, Berks, UK). Ultrathin sections (75 nm) were mounted on copper grids and stained with uranium acetate and lead citrate. The sections were observed using an H-7000 electron microscope (Hitachi, Tokyo, Japan). Morphometric analysis of mitochondria was performed by measuring average percentage of area occupied by cristae within a mitochondrion at the inner segment.

Statistical Analysis

In statistical analysis of thickness of retinal layers and TUNEL-positive cells, three wild-type and four *Uchl3*-deficient mice were used in each time point (P0, P10, 3w,

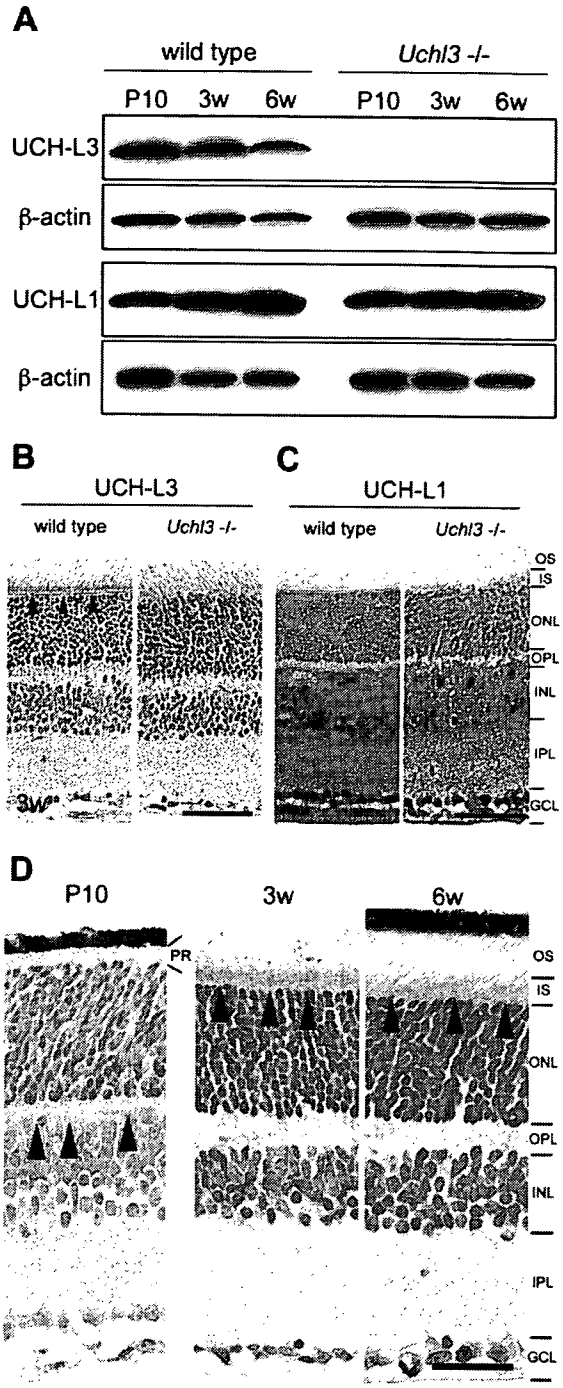

Figure 1. Expression of UCH-L1 and UCH-L3 in the retina of wild-type and *Uchl3*-deficient mice. **A:** Western blot analysis of UCH-L3 and UCH-L1 using whole-eye lysates from wild-type and *Uchl3*-deficient mice at P10, 3w, and 6w. The immunoreactive band for UCH-L3 is undetectable in *Uchl3*-deficient mice. Expression of UCH-L1 is similar between both genotypes. **B** and **C:** Immunohistochemistry for UCH-L3 (**B**) and UCH-L1 (**C**) in wild-type and *Uchl3*-deficient mice retinae at 3w. Immunoreactivity of UCH-L3 is found at the inner segment of the wild-type retina (**arrowheads**), whereas there is no significant immunoreactivity in *Uchl3*-deficient mice (**B**). UCH-L1 is expressed at the inner retina in both genotypes. **D:** Immunohistochemistry of UCH-L3 at P10, 3w, and 6w in wild-type retinae. UCH-L3 is faintly expressed in the outer plexiform layer at P10 (**arrowheads**). Thereafter, immunoreactivity for UCH-L3 is found in inner segment at 3w and 6w (**arrowheads**). PR, photoreceptor; OS, outer segment; IS, inner segment; ONL, outer nuclear layer; OPL, outer plexiform layer; INL, inner nuclear layer; IPL, inner plexiform layer; GCL, ganglion cell layer. Scale bars = 50 μm (**B** and **C**) and 20 μm (**D**).

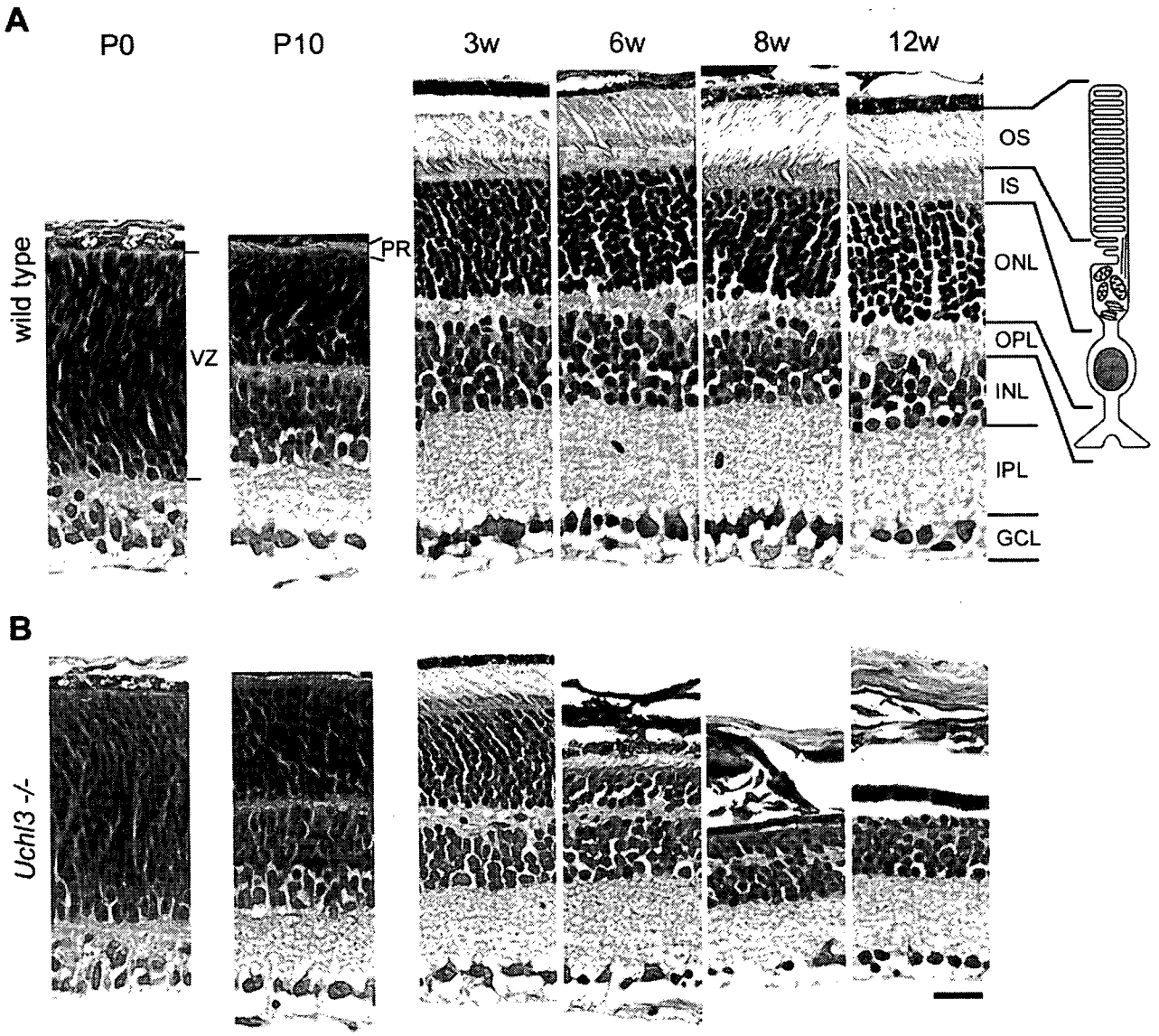

Figure 2. Histopathological changes of postnatal development in wild-type (**A**) and retinal degeneration of *Uchl3*-deficient mice (**B**) at P0, P10, 3w, 6w, 8w, and 12w. There is no morphological difference between both genotypes at P0 and P10, whereas outer and inner segments, outer nuclear layers, and outer plexiform layers are progressively degenerated after 3w of age. The illustration indicates a rod photoreceptor cell. VZ, ventricular zone; PR, photoreceptor; OS, outer segment; IS, inner segment; ONL, outer nuclear layer; OPL, outer plexiform layer; INL, inner nuclear layer; IPL, inner plexiform layer; GCL, ganglion cell layer. H&E staining. Scale bar = 20 μm (**A** and **B**).

6w, 8w, and 12w; for a total of 42 mice). The percentage of cristae area to whole mitochondrion in ultramicrophotographs was measured in 50 mitochondria of each genotype from three wild-type mice and four *Uchl3*-deficient mice, and the data were subjected to statistical analysis. All statistical analyses were carried out by Student's *t*-test using Microsoft Excel.

Results

Expression of UCH-L3 in the Murine Retina

Western blotting detected UCH-L3 (~30 kd) in extracts of eyes from wild-type mice at P10, 3w, and 6w, but the band was undetectable in *Uchl3*-deficient mice (Figure 1A). The expression level of UCH-L1 was similar in both genotypes. There was a tendency that the level of UCH-L3 decreased with age while the level of UCH-L1 increased with age in wild-type mice of all samples examined (five blots per antibody). Immunohistochemically, the cellular distribution of UCH-L3 differed from that of UCH-L1. UCH-L3 was enriched in the photoreceptor inner segment in wild-type mice at 3w of age (Figure 1B), whereas UCH-L1 was expressed in both genotypes in the inner retina, which consists of the inner nuclear layer, inner plexiform layer, and ganglion cell layer (Figure 1C). Localization of UCH-L3 in the wild-type retina was altered with age (Figure 1D). Immunoreactivity for UCH-L3 was not found at P0. UCH-L3 was faintly expressed in the outer plexiform layer at P10. Thereafter, it was localized to